JACS
JOURNAL OF THE AMERICAN CHEMICAL SOCIETY
Article
pubs.acs.org/JACS

Atmospheric Chemistry of Criegee Intermediates: Unimolecular Reactions and Reactions with Water

Bo Long,[†,‡] Junwei Lucas Bao,[‡] and Donald G. Truhlar*[,‡]

[†]College of Information Engineering, Guizhou Minzu University, Guiyang 550025, China

[‡]Department of Chemistry, Chemical Theory Center, and Supercomputing Institute, University of Minnesota, Minneapolis, Minnesota 55455-0431, United States

Supporting Information

ABSTRACT: Criegee intermediates are produced in the ozonolysis of unsaturated hydrocarbons in the troposphere, and understanding their fate is a prerequisite to modeling climate-controlling atmospheric aerosol formation. Although some experimental and theoretical rate data are available, they are incomplete and partially inconsistent, and they do not cover the tropospheric temperature range. Here, we report quantum chemical rate constants for the reactions of stabilized formaldehyde oxide (CH_2OO) and acetaldehyde oxide (*syn*-CH_3CHOO and *anti*-CH_3CHOO) with H_2O and for their unimolecular reactions. Our results are obtained by combining post-CCSD(T) electronic structure benchmarks, validated density functional theory potential energy surfaces, and multipath variational transition state theory with multidimensional tunneling, coupled-torsions anharmonicity, and high-frequency anharmonicity. We consider two different types of reaction mechanisms for the bimolecular reactions, namely, (i) addition-coupled hydrogen transfer and (ii) double hydrogen atom transfer (DHAT). First, we show that the MN15-L exchange-correlation functional has kJ/mol accuracy for the $CH_2OO + H_2O$ and *syn*-$CH_3CHOO + H_2O$ reactions. Then we show that, due to tunneling, the DHAT mechanism is especially important in the *syn*-$CH_3CHOO + H_2O$ reaction. We show that the dominant pathways for reactions of Criegee intermediates depend on altitude. The results we obtain eliminate the discrepancy between experiment and theory under those conditions where experimental results are available, and we make predictions for the full range of temperatures and pressures encountered in the troposphere and stratosphere. The present results are an important cog in clarifying the atmospheric fate and oxidation processes of Criegee intermediates, and they also show how theoretical methods can provide reliable rate data for complex atmospheric processes.

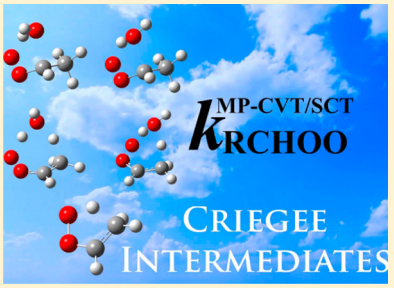

1. INTRODUCTION

Criegee intermediates[1] are carbonyl oxides formed in the ozonolysis of unsaturated hydrocarbons; their atmospheric fate plays a critical role in determining the oxidative efficacy of the atmosphere and its capacity for free radical generation and secondary organic aerosol formation.[2−5] In the atmosphere, Criegee intermediates undergo bimolecular reactions with atmospheric molecules such as H_2O, SO_2, and HCOOH and unimolecular isomerization and decomposition to yield OH.[2] Inferences about the roles of Criegee intermediates were originally based on indirectly estimated rate constants, and there has been no consensus on whether the dominant reaction of stabilized Criegee intermediates in the troposphere is with water molecules.[2,6] Furthermore, the unimolecular reactions of Criegee intermediates must be considered when estimating the atmospheric fate of Criegee intermediates and the production of atmosphere-cleansing OH.[7−9] In addition to their role as sources of OH, exploring the reactions of Criegee intermediates with water and their unimolecular reactions is especially critical because of the abundance of water in the atmosphere and because the bimolecular reactions of stabilized Criegee intermediates in the atmosphere are key processes in the formation of aerosols,[10,11] which scatter sunlight and affect earth's radiative balance.[8,9] In particular, the oxidation of sulfur dioxide via stabilized Criegee intermediates is an important source of sulfuric acid,[12−18] which plays an important role in aerosol nucleation.

Given the importance of Criegee intermediates, it is very exciting that new experimental methods have been developed to directly measure bimolecular rate constants for reactions of stabilized Criegee intermediates with atmospheric compounds.[19−25] Elucidating the kinetics of bimolecular reactions between Criegee intermediates and atmospheric molecules and the kinetics of their unimolecular reactions is essential for fully estimating the atmospheric fates of Criegee intermediates and for making chemical models of the atmosphere more reliable.

However, direct rate constant data for the reactions of Criegee intermediates with H_2O are still scarce and are partially inconsistent. Moreover, the rate constants of their unimolecular reactions are even more limited and complicated because they depend on temperature and pressure. Throughout this article, we will give rate constants in units of cm^3 $molecule^{-1}$ s^{-1} and s^{-1} for bimolecular and unimolecular reactions, respectively.

Received: August 18, 2016
Published: September 29, 2016

DOI: 10.1021/jacs.6b08655
J. Am. Chem. Soc. 2016, 138, 14409−14422

Welz et al.[20] estimated the $CH_2OO + H_2O$ reaction rate constant as $<4 \times 10^{-15}$, Chao et al.[26] estimated $<1.5 \times 10^{-15}$, Stone et al.[27] measured 5.4×10^{-18} at 297 K, Ouyang et al.[28] measured $(2.5 \pm 1) \times 10^{-17}$ at 297 K, and Newland et al.[29] measured $(1.3 \pm 0.4) \times 10^{-15}$ at 298 K. The kinetic data is even more limited with regard to distinguishing the reactions of *syn*-CH_3CHOO and *anti*-CH_3CHOO with H_2O. The suggested upper limit rate constant for the *syn*-$CH_3CHOO + H_2O$ reaction is $<4 \times 10^{-15}$ by Taatjes et al.[30] and $<2 \times 10^{-16}$ by Sheps et al.,[31] whereas the experimental rate constant for the *anti*-$CH_3CHOO + H_2O$ reaction by Taatjes et al.[30] is $(1.0 \pm 0.4) \times 10^{-14}$. The main reason for the uncertainties in the experimental kinetics data is the efficient reactions of Criegee intermediates with water dimer. With regard to their unimolecular reactions, there are different values due to different temperatures and pressures. For example, the experimental unimolecular rate constant of CH_2OO is reported to be 8.8 ± 13 at 298 K,[29] while the upper limit rate constant is estimated to be 11.6 ± 8 at 293 K at low pressure between 7 and 30 Torr.[32] However, other experimental results are 115 ± 20 at 295 K and 5.1 Torr[33] and 73−283 at 297 K and 100 Torr.[34] As summarized elsewhere,[35] the experimental unimolecular rate constants of *syn*-CH_3CHOO extend over an even larger range: 2.5−250. Furthermore, there have not been any experimental data reported for the unimolecular rate constant of *anti*-CH_3CHOO.

Absolute rate constants can also be obtained by theory, but theoretical rate constants are quite sensitive to the electronic structure calculations of barrier heights, which span a wide range. For example, CCSD(T)/aug-cc-pVTZ//B3LYP/6-311++G(2df,2p) calculations give a barrier of 1.5 kcal for the $CH_2OO + H_2O$ reaction,[36] whereas the barrier height is estimated to be 2.82 kcal by QCISD(T)/CBS//B3LYP/6-311++G(2d,2p).[39] (All energetic and enthalpic quantities in the whole article are molar quantities, and we use kcal as the unit for energy per mole.) An important aspect of the difficulty of the calculations is that the electronic structure of Criegee intermediates is inherently multiconfigurational. The uncertainties in the barrier height due to the difficulty in treating inherently multiconfigurational systems probably account for much of the large differences[6,36−39] between recent experimental kinetic data and available theoretical studies of bimolecular reactions of Criegee intermediates with H_2O. In addition to the incompleteness of the electronic structure methods employed (i.e., their deviations from complete configuration interaction), there are uncertainties due to the previous theoretical dynamics calculations[38,39] being based on conventional transition state theory and very approximate calculations of the tunneling contributions. Higher-accuracy theoretical methods for both electronic structure and dynamics are needed to estimate reliable reaction kinetics for the bimolecular reactions between Criegee intermediates and H_2O and their unimolecular reactions, and such higher-level theory is used in the present study.

For the electronic structure, we need wave function theory (WFT) at a higher level than CCSD(T),[40] and we will utilize the recently developed W3X[41] and W3X-L[42] efficient composite methods to include beyond-CCSD(T) effects. We will use these to obtain reference data, and we will use this reference data to validate the use of a density functional theory (DFT) exchange-correlation functional that has a low enough cost to be used for reasonably complete direct dynamics calculations of the rate constants. By reasonably complete, we mean that the dynamics calculations include variational location of the transition state, multipath multidimensional tunneling, multiple-structure anharmonicity, and torsional-potential and high-frequency anharmonicity.

We consider the following reactions:

$$CH_2OO + H_2O \rightarrow CH_2(OH)OOH \quad \text{(B1a)}$$

$$CH_2OO \rightarrow \quad \text{(U1c)}$$

$$CH_2OO \rightarrow HCO + OH \quad \text{(U1d)}$$

$$CH_2OO + H_2O \rightarrow HCO + OH + H_2O \quad \text{(B1dh)}$$

$$syn\text{-}CH_3CHOO + H_2O \rightarrow HC(OH)CH_3OOH \quad \text{(B2a)}$$

$$syn\text{-}CH_3CHOO + H_2O \rightarrow CH_2{=}CHOOH + H_2O \quad \text{(B2dh)}$$

$$syn\text{-}CH_3CHOO \rightarrow CH_2{=}CHOOH \quad \text{(U2hs)}$$

$$syn\text{-}CH_3CHOO \rightarrow \quad \text{(U2c)}$$

$$anti\text{-}CH_3CHOO + H_2O \rightarrow HC(OH)CH_3OOH \quad \text{(B3a)}$$

$$anti\text{-}CH_3CHOO \rightarrow \quad \text{(U3c)}$$

$$anti\text{-}CH_3CHOO \rightarrow CH_3CO + OH \quad \text{(U3d)}$$

Reactions B1a, B2a, and B3a are bimolecular (B) addition (a) reactions accompanied by hydrogen transfer of water to the peroxyl group and will be called addition-coupled hydrogen-atom transfer (ACHAT). U1c, U2c, and U3c are unimolecular (U) cyclizations (c). Reactions U1d and U3d are unimolecular decomposition (d) reactions catalyzed by water, and they are special cases of the class of reactions known[43] as double hydrogen-atom transfer (DHAT); B1dh and B2dh are DHAT reactions (dh) occurring in bimolecular collisions catalyzed by water. U2hs is a unimolecular 1,4-hydrgen shift reaction.

The present results not only give reliable rate constants for the reactions between Criegee intermediates and H_2O and for their unimolecular reactions but also provide insights into the methodological requirements for calculating theoretical rate constants with experimental accuracy for atmospheric reactions. In addition, we also provide a new insight into how the dominant atmospheric reaction processes of Criegee intermediates vary with altitude, depending on temperature and pressure. Therefore, the results in this article are of interest both for atmospheric chemistry and for computational chemistry.

2. COMPUTATIONAL METHODS

2.1. Electronic Structure. To obtain quantitatively reliable rate constants at atmospheric temperatures, the errors in electronic structure calculations must be a few tenths of a kcal or less. This is particularly difficult for systems with large nondynamic correlation. We tested the stability of singlets using the *Gaussian 09* keyword (stable=opt) found that CH_2OO is best described as a closed-shell singlet. The extent of nondynamic correlation can be gauged by the T_1 diagnostic; for closed-shell systems, a T_1 diagnostic greater than 0.02 is considered to be an indication of large nondynamic correlation.[44] We calculated T_1 diagnostics of 0.046−0.048, 0.036−0.040, and 0.037−0.42 for CH_2OO, *syn*-CH_3CHOO, and *anti*-CH_3CHOO, respectively, where the range indicates values obtained with different basis sets, and we calculated a T_1 diagnostic of 0.026 for the transition state of reaction B1a. We conclude that nondynamic correlation energy is

DOI: 10.1021/jacs.6b08655
J. Am. Chem. Soc. 2016, 138, 14409−14422

large, and we must examine high-order methods if we are to have confidence in the results.

To learn what level of theory is needed to attain the required accuracy, we performed benchmark calculations of beyond-CCSD(T) accuracy. Chan and Radom[41,42] developed the W2X composite WFT method as an economical approximation to CCSD(T)/CBS, where CBS denotes a complete basis set, and they developed W3X and W3X-L (where W3X-L uses a larger basis sets than W3X) as efficient composite WFT approximations for estimating CCSDT(Q)/CBS. The accuracy of W3X-L is estimated to be on the order of a few tenths of a kcal. In the original W2X, W3X, and W3X-L methods, calculations are carried out at geometries optimized using the B3LYP exchange-correlation functional; in the present work, we used higher-level geometries obtained by restricted CCSD(T)-F12a/TZ-F12,[45−47] restricted CCSD(T)-F12a/DZ-F12, and restricted QCISD/TZ,[48] for closed-shell systems and by unrestricted CCSD(T)-F12a/TZ-F12,[45−47] unrestricted CCSD(T)-F12a/DZ-F12, and unrestricted QCISD/TZ[48] for open-shell doublet systems, where the shorthand notation "XZ" with X = D or T is used for "cc-pVXZ" in the names or parts of the names of correlation-consistent[49,50] basis sets.

First, we studied the simplest Criegee intermediate (CH_2OO) and the transition structures and products for its reaction with H_2O and its unimolecular reactions. All reactants, precursor complexes, transition states, and products were optimized by QCISD/TZ. The frequencies of these stationary points were calculated at the same level to confirm that the equilibrium structures do not have any imaginary frequencies and a transition state has only one imaginary frequency. We then optimized the geometries and calculated the vibrational frequencies using all three WFT methods specified above. Single-point energies were then calculated using the W3X-L and W3X composite methods based on these geometries.

As candidates for including dynamic calculations, we tested three exchange-correlation functionals, namely, MN15-L,[51] M11-L,[52] and M06-L;[53] we used the MG3S[54] and maug-TZ[55] basis sets. In addition, minimum-energy paths (MEPs) were calculated by MN15-L/MG3S to examine whether the given transition state connects with the corresponding reactant and product (see Figures S1−S15, Supporting Information). We utilized a very fine grid with 225 radial shells around each atom and 974 angular points in each shell in the density functional calculations. Frequencies were computed to confirm the nature of every stationary point.

Then, we studied reactions of the higher homologues, and, as specified below, we used a subset of the methods explained above.

The electronic structure calculations were executed using the *Gaussian 09*,[56] *MN-GFM*,[57] *Molpro 2012*,[58] and *MRCC*[59,60] electronic structure codes.

2.2. Thermodynamic and Activation Quantities. Throughout the discussion, we label differences in Born−Oppenheimer potential energy at equilibrium and transition structures as "energy" E; relative to reactants, this gives energies of reaction when comparing products to reactants and classical barrier heights when comparing transition states to reactants. Adding zero-point energy to the potential energy gives H_0°, the enthalpy at 0 K, and differences in enthalpy at stationary points may be either enthalpy of reaction or conventional transition state theory enthalpy of activation. All enthalpic quantities in the entire article are given for 0 K. Rate constants require free energies, G_T°, at temperature T, and in the present work, the quantities we use are free energies of activation calculated as variational transition state free energy minus reactant free energy.

In calculating enthalpies and energies, scale factors[61] listed in Table S1 were applied to all directly calculated harmonic vibrational frequencies (this improves the zero-point energies by including both anharmonicity and systematic error correction for the high frequencies[61]), and all finite-T results employed the multistructural method with torsional anharmonicity (MS-T).[62−65] (this includes the energetic and entropic effects of multiple conformations and coupled-torsional-potential anharmonicity).

2.3. Kinetics. The rate constants were calculated using multipath canonical variational transition state theory with small curvature tunneling (MP-CVT/SCT).[66−70] We included all reaction paths (i.e., paths through each of the saddle points, when there is more than one parallel path), except where it is explicitly noted that a higher-energy transion structure is not included in the kinetics. Rate constants were calculated using the *Polyrate 2010A*[71] and *Gaussrate 2009*[72] dynamics codes. The pressure-dependent bimolecular and unimolecular isomerization rate constants are computed using our recently proposed nonempirical system-specific quantum RRK theory (SS-QRRK) with the Lindemann−Hinshelwood mechanism for unimolecular isomerization and chemical activation mechanism for bimolecular association.[73−75] The critical energy parameters of the SS-QRRK treatment are set equal to the high-pressure-limit temperature-dependent Arrhenius activation energies computed from the fitting formula (see Section 3.3) for the rate constants. Lennard-Jones parameters, σ and ε/k_B, for CH_3CHOO are 5.39 Å and 423 K;[76] for CH_2OO, they are 3.79 Å and 520 K;[77] and for the bath gas N_2, they are 3.74 Å and 82 K.[76] The average energy transferred per deactivating collision is taken to be $\langle \Delta E \rangle_{down} = 200(T/300)^{0.85}$ cm^{-1}, which has been used in previous atmospheric modeling.[78] (In the literature, $\langle \Delta E \rangle_{down}$ is called the average energy transferred per deactivating collision, which means that it is the average energy transferred in collisions in which the internal energy of the activated molecule decreases. Note that $\langle \Delta E \rangle_{down}$ is a positive number, and it should not be confused with $\langle \Delta E \rangle_{all}$, which is the average energy transferred in both up and down energy transfer collisions and is negative.) The F_E parameter is computed by the Whitten−Rabinovitch method.[79]

The pressure dependence considered here neglects the small fraction of unstabilized Criegee intermediates that would be formed at low pressure.

For B1a, the high-pressure limit rate constant is calculated by multipath variational transition state theory with small-curvature tunneling with the MN15-L/MG3S potential energy surface. For U1c, B2a, B2dh, U2hs, B3a, and U3c, the high-pressure limit rate constant is calculated as

$$k = \frac{k_{\text{MS-TST}}^{\text{HL}}}{k_{\text{MS-TST}}^{\text{LL}}} k_{\text{MP-CVT/SCT}}^{LL} \quad (1)$$

where MP-CVT/SCT denotes multipath variational transition state theory with small-curvature tunneling, MS-TST denotes a multistructural transition state theory calculation without tunneling and without variational optimization of the transition state, and LL and HL denote lower and higher levels of electronic structure theory, respectively. In cases studied here, LL is MN15-L/maug-TZ, whereas HL is W3X-L//QCISD/TZ for B2a, B2dh, and B3a and W3X-L//CCSD(T)-F12a/DZ-F12 for U1c, U2hs, and U3c. We did not calculate the rate constants of U1d, B1dh, U2c, and U3d because their barrier heights are too high to make a significant contribution.

For interpretive purposes, it is useful to consider the contributions of each reaction path to an overall rate constant; this is done as follows. A transition state is a $(3N - 7)$-dimensional hypersurface separating reactants from products, where N is the number of atoms. A multistructural transition state is a multifaceted transition state with each facet being normal to a reaction path through one of the transition structures, where the transition structures are saddle points with one imaginary frequency; the expression for the MP-CVT/SCT rate constant can be rearranged and written as a sum over contributions from each facet.[68] Having done this, we can define F_j as the fractional contribution of reaction path j to the overall rate.

To compare bimolecular (B) reaction rates with water to unimolecular (U) reaction rates, it is useful to convert the bimolecular reaction rate constants to pseudo-first-order (P1) reaction rate constants by

$$k_{P1} = k_B[H_2O] \quad (2)$$

where $[H_2O]$ is the concentration of water. Then, the respective reaction-specific lifetimes for disappearance by bimolecular reaction with water and by unimolecular reaction are the reciprocals of k_{P1} and k_U. (One should not confuse the reaction-specific lifetime with the overall lifetime due to all possible reactions.) In the Results and Discussion section, we will also use the analog of eq 2 to compute

DOI: 10.1021/jacs.6b08655
J. Am. Chem. Soc. 2016, 138, 14409−14422

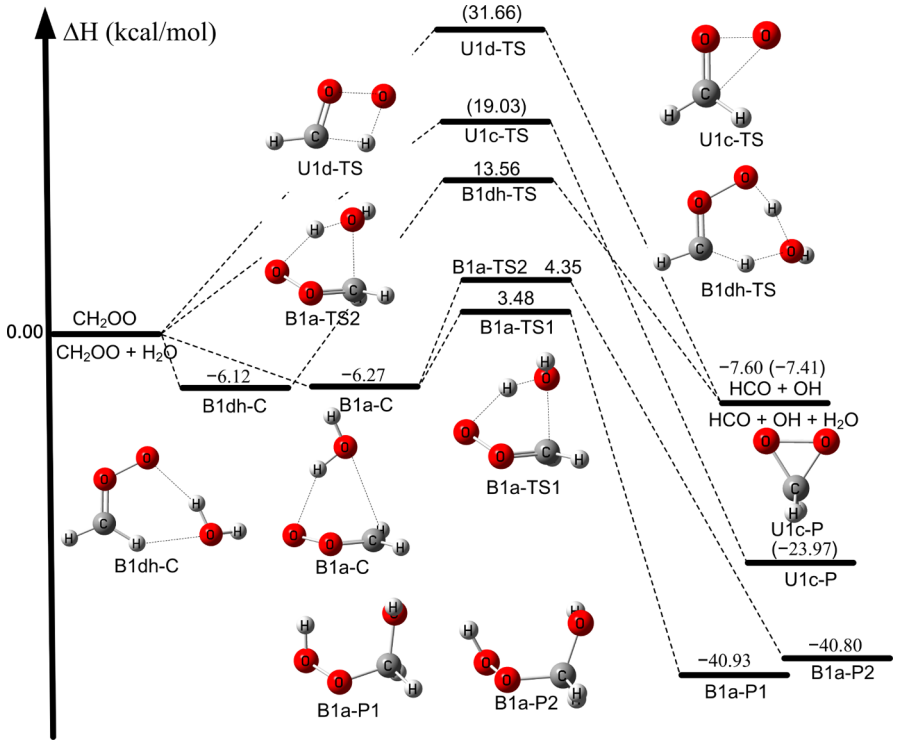

Figure 1. Enthalpies for the reactants, intermediates, transition structures, and products of the $CH_2OO + H_2O$ reaction (ACHAT reaction 1a, which may occur by either of the bottom two paths) and the unimolecular reaction of CH_2OO (reaction 1b, which is the top path), as calculated by W3X-L//QCISD/TZ and W3X-L//CCSD(T)-F12a/DZ-F12 (in parentheses).

pseudo-first-order (P1) reaction rate constants for reaction with water dimer.

3. RESULTS AND DISCUSSION

3.1. Electronic Structure and Enthalpies of Activation for Reaction of CH_2OO with H_2O. The electronic structure of CH_2OO has been classified as a biradical[80] or zwitterion.[21,81−83] The bond lengths of the critical bonds and the rotational constants of CH_2OO for optimized structures are given in Tables S2 and S3. Table S3 also contains experimental[84] rotational constants; the calculations agree reasonably well with experiments. Using MN15-L/MG3S, we calculated the bond lengths for the critical C−O and O−O bonds of CH_2OO to be 1.260 and 1.342 Å (see Table S2); these values agree well with the values of 1.26−1.27 and 1.40−1.43 Å obtained in previous work with other methods.[85−87]

The vibrational frequencies of CH_2OO calculated by various methods are provided in Tables S4 and S5, where they are compared to experiment. This comparison shows that the scaled MN15-L frequencies are accurate enough results to use for dynamics calculations.

Although the $CH_2OO + H_2O$ reaction has been studied before,[36,39,38,39,88,76,89] the present investigation includes previously neglected structures. For the $CH_2OO + H_2O$ reaction and the CH_2OO unimolecular reactions, we consider the reaction pathways in Figure 1, which shows the bimolecular ACHAT and DHAT reactions B1a and B1dh and the unimolecular isomerizations U1c and U1d. We find that the two bimolecular reactions start with the formation of a complex with two conformations, B1a-C and B1dh-C (shown in Figure 1). Previously, the only complex considered was B1dh-C,[36,39,39] but our CCSD(T)-F12a/TZ-F12 calculations (given in Table S6) show that two complexes should be considered; B1a-C and B1dh-C are both low in energy, with B1a-C being slightly lower. Note that experimental rotational constants are available only for B1dh-C,[90] as listed in Table S3.

After passing through the complexes, the bimolecular reaction then proceeds through a multifaceted transition state with three transition structures (saddle points): B1a-TS1, B1a-TS2, and B1dh-TS in Figure 1; these transition structures form either the $CH_2(OH)OOH$ association product with two conformations, B1a-P1 and B1a-P2, of reaction B1a or the dissociation products HCO + OH, which are the same as the products of reaction U1d. We found that the reaction pathway for ACHAT involves two transition structures (differing in the orientation of the free OH group in H_2O, as shown in Figure 1), whereas previous calculations included only one.[36,88,76] The existence of multiple low-energy structures mainly affects the entropies and free energies, with little effect on enthalpies. The contribution of B1a-TS2 should not be neglected because B1a-TS2 is calculated by W3X-L//QCISD/TZ to have an enthalpy of activation only 0.87 kcal higher than B1a-TS1. Although DHAT processes have been known for a long time[91−94] and are important in many atmospheric processes,[43,95−99] in the present case the enthalpy of activation of water-assisted DHAT of CH_2OO via B1dh-TS is computed by W3X-L//QCISD/TZ to be 13.70 kcal, which is 9.35 kcal higher than reaction via B1a-TS2 and 10.22 kcal higher than reaction via B1a-TS1, as shown in Figure 1. We conclude that the DHAT process is negligible for the $CH_2OO + H_2O$ reaction. Thus, we consider only transition structures B1a-TS1 and B1a-TS2 for reaction rate constant calculations.

Barrier heights calculated by several methods are given in Table S7. The MN15-L/MG3S barrier heights of B1a-TS1 and B1a-TS2 are 0.51 and 1.52 kcal, respectively, which are in excellent agreement with the values of 0.49 and 1.45 kcal

DOI: 10.1021/jacs.6b08655
J. Am. Chem. Soc. 2016, 138, 14409−14422

obtained with our most accurate calculation, W3X-L//CCSD(T)-F12a/TZ-F12. When the zero-point contribution is added, the MN15-L/MG3S conventional transition state theory enthalpies of activation for B1a-TS1 and B1a-TS2 are 3.25 and 4.12 kcal, respectively, and these agree well with the W3X-L//CCSD(T)-F12a//TZ-F12 values of 3.52 and 4.37 kcal, as shown in Table 1. The mean unsigned error (MUE) of MN15-L/MG3S is even lower than that of W2X//CCSD(T)-F12a/TZ-F12. These results show that the MN15-L functional has the required accuracy for a quantitative treatment of the $CH_2OO + H_2O$ reaction.

Table 1. Conventional Transition State Theory Enthalpies of Activation $\Delta H_0^{\ddagger,\circ}$ for the Bimolecular Reactions (in kcal)

methods	$\Delta H_0^{\ddagger,\circ}$		MUE[a]
	B1a-TS1	B1a-TS2	
W3X-L//CCSD(T)-F12a/TZ-F12	3.52	4.37	0.00
W3X-L//CCSD(T)-F12a/DZ-F12	3.51	4.39	0.02
W3X-L//QCISD/TZ	3.48	4.35	0.03
W3X//QCISD/TZ	3.43	4.27	0.10
MN15-L/MG3S	3.25	4.12	0.26
W2X//CCSD(T)-F12a/TZ-F12	2.99	3.82	0.54
W2X//CCSD(T)-F12a/DZ-F12	2.98	3.84	0.54
W2X//QCISD/TZ	2.87	3.74	0.64
	B2a-TS1	B2a-TS2	
W3X-L//QCISD/TZ	7.53	8.89	0.00
W3X//QCISD/TZ	7.48	8.80	0.07
MN15-L/maug-TZ	7.84	9.23	0.33
W2X//QCISD/TZ	7.04	8.39	0.50
	B2dh-TS1	B2dh-TS2	
W3X-L//QCISD/TZ	9.68	9.87	0.00
W3X//QCISD/TZ	9.28	9.47	0.40
W2X//QCISD/TZ	9.19	9.39	0.49
MN15-L/maug-TZ	10.81	10.89	1.08
	B3a-TS1	B3a-TS2	
W3X-L//QCISD/TZ	1.18	1.77	0.00
W3X//QCISD/TZ	1.04	1.61	0.15
MN15-L/maug-TZ	1.75	2.24	0.52
W2X//QCISD/TZ	0.55	1.14	0.63

[a]Mean unsigned error averaged over the two previous columns.

Our best theoretical method, W3X-L//CCSD(T)-F12a//TZ-F12, yields 3.52 and 4.37 kcal, respectively, for the enthalpies of activation of B1a-TS1 and B1a-TS2; these values are about 0.7 kcal higher than those[39] obtained in previous work by QCISD(T)/CBS//B3LYP/6-311+G(2d,2p). This result and other calculations in Tables S7 and 1 show that going beyond CCSD(T) is important for quantitative accuracy.

Tables 1 and S7 show that the much more affordable W3X-L//QCISD/TZ method agrees with W3X-L//CCSD(T)-F12a/TZ-F12 within a few hundredths of a kcal. Given the huge computational cost of W3X-L//CCSD(T)-F12a/TZ-F12 for larger molecules, we chose the W3X-L//QCISD/TZ theoretical method as the benchmark method for the bimolecular reactions. Furthermore, MN15-L with the larger maug-TZ basis set is selected for dynamics in the larger systems.

3.2. Unimolecular Reaction of CH_2OO. The unimolecular reaction of CH_2OO occurs via two different reaction mechanisms: hydrogen transfer and the oxygen transfer, as shown in Figure 1. The W3X-L//CCSD(T)-F12a/DZ-F12 calculations show that the enthalpy of activation for the oxygen transfer (U1c) via U1c-TS is 12.63 kcal lower than that of the hydrogen transfer via U1d-TS. Therefore, we consider only U1c-TS for dynamics calculations.

Table 2 shows that the enthalpies of activation of U1c-TS and U1d-TS are computed to be 19.03 and 31.66 kcal at the W3X-L//CCSD(T)-F12a/DZ-F12 level, which are in excellent agreement with the corresponding values of 19.1 and 31.8 kcal by HEAT-345(Q).[100] In addition, the enthalpy of reaction U1d is computed to be −7.41 kcal by W3X-L//CCSD(T)-F12a/DZ-F12; this is in good agreement with the value of −7.4 kcal by HEAT-345(Q).[100] Additionally, Table 2 shows that the MUE (relative to our best calculation) of W3X-L//CCSD(T)-F12a/DZ-F12 is only 0.01 kcal, whereas that of W3X-L//QCISD/TZ MUE is 0.12 kcal. Thus, we chose the W3X-L//CCSD(T)-F12a/DZ-F12 theoretical method as the benchmark method for the unimolecular reactions.

Table 2. Conventional Transition State Theory Enthalpies of Activation $\Delta H_0^{\ddagger,\circ}$ for the Unimolecular Reactions (in kcal)

methods	$\Delta H_0^{\ddagger,\circ}$		MUE
	U1c-TS	U1d-TS	
W3X-L//CCSD(T)-F12a/TZ-F12	19.03	31.64	0.00
W3X-L//CCSD(T)-F12a/DZ-F12	19.03	31.66	0.01
W3X-L//QCISD/TZ	18.87	31.57	0.12
W2X//QCISD/TZ	18.91	31.12	0.32
W2X//CCSD(T)-F12a/DZ-F12	19.29	31.24	0.33
W2X//CCSD(T)-F12a/TZ-F12	19.30	31.22	0.35
MN15-L/maug-TZ	20.00	31.26	0.68
	U2hs-TS	U2c-TS	
W3X-L//CCSD(T)-F12a/DZ-F12	17.01	23.70	0.00
W2X//CCSD(T)-F12a/DZ-F12	16.57	24.04	0.39
MN15-L/maug-TZ	16.41	23.91	0.41
	U3c-TS	U3d-TS	
W3X-L//CCSD(T)-F12a/DZ-F12	15.63	29.01	0.00
MN15-L/maug-TZ	16.18	28.98	0.29
W2X//CCSD(T)-F12a/DZ-F12	15.86	28.50	0.37

3.3. Electronic Structure of *syn*-CH_3CHOO and *anti*-CH_3CHOO and the Transition States for Reaction with H_2O. Methyl substitution of CH_2OO yields two isomers, *syn*-CH_3CHOO and *anti*- CH_3CHOO. Calculations by W3X-L//QCISD/TZ show that *syn*-CH_3CHOO is more favorable than *anti*-CH_3CHOO by about 3.3 kcal as shown in Figure S16, which is consistent with the previous theoretical results.[76,101,102] Figure S16 also shows that the transformation of *anti*-CH_3CHOO to *syn*-CH_3CHOO has a 38.50 kcal enthalpy of activation, which indicates that the unimolecular interconversion between *syn*-CH_3CHOO and *anti*-CH_3CHOO is negligible in the atmosphere; therefore, *anti*-CH_3CHOO and *syn*-CH_3CHOO are treated as independent reactants. The 38.50 kcal enthalpy of activation of the unimolecular interconversion between *syn*-CH_3CHOO and *anti*-CH_3CHOO is about 4 kcal higher than that of the previous investigation[76] by MCG3[103]//QCISD/MG3. This result again indicates that beyond-CCSD(T) theoretical methods are necessary for quantitative work on Criegee intermediates.

The calculated rotational constants of *syn*-CH_3CHOO by MN15-L/maug-TZ are in excellent agreement with experiment and coupled cluster theory, as shown in Table S8.[101,104]

For Criegee intermediates with methyl groups, a hydrogen atom of the methyl group is transferred to the terminal oxygen atom, which is of great importance in the atmosphere because

DOI: 10.1021/jacs.6b08655
J. Am. Chem. Soc. 2016, 138, 14409−14422

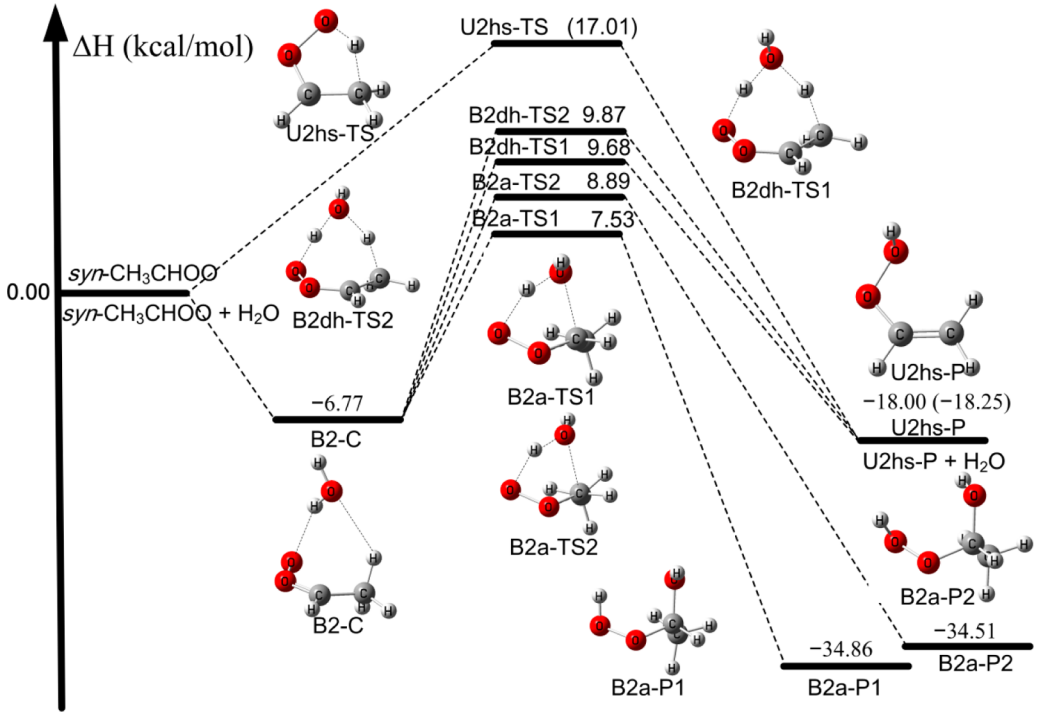

Figure 2. Enthalpies for the reactants, intermediates, transition states, and products of the *syn*-CH_3CHOO + H_2O reaction and the unimolecular reaction of *syn*-CH_3CHOO, as calculated by W3X-L//QCISD/TZ and W3X-L//CCSD(T)-F12a/DZ-F12 (in parentheses). Note that the product of reaction B2dh is labeled U2hs-P + H_2O.

this process could lead to the formation of OH.[78,105−107] Although the reaction mechanisms of *syn*-CH_3CHOO and *anti*-CH_3CHOO with H_2O are similar to that of the CH_2OO + H_2O reaction, as illustrated in Figures 2 and S17, the DHAT processes are not negligible in the *syn*-CH_3CHOO + H_2O reaction because the enthalpies of activation of the ACHAT process via B2a-TS1 and B2a-TS2 are only about 1−2 kcal lower than those of DHAT processes via B2dh-TS1 and B2dh-TS2 in Table 1 and Figure 2. However, previous investigations only took into account the ACHAT process.[36,39,76] In the present work, we consider four reaction channels in the *syn*-CH_3CHOO + H_2O reaction. For the *anti*-CH_3CHOO + H_2O reaction, we consider only the ACHAT process (with two reaction pathways) because the DHAT process involves the hydrogen atom of the CHOO group in *anti*-CH_3CHOO migrating to the terminal oxygen atom of *anti*-CH_3CHOO, but this is similar to the process in CH_2OO + H_2O that has a high barrier.

Table 1 shows that the MUE of W3X//QCISD/TZ is only 0.07 kcal for B2a. This validates W3X//QCISD/TZ for this ACHAT processes. The enthalpies of activation for transition states B2a-TS1 and B2a-TS2 calculated by W3X-L//QCISD/TZ are about 0.7 kcal higher than that calculated[39] by QCISD/CBS//B3LYP/6-311++G(2d,2p).

In Table 1, W3X-L//QCISD/TZ benchmark calculations indicate that the results obtained by MN15-L/maug-TZ are again very accurate for the ACHAT process. In particular, the MN15-L/maug-TZ conventional transition state theory enthalpies of activation of B2a-TS1 and B2a-TS2 are calculated to be 7.84 and 9.23 kcal, which are only 0.31 and 0.34 kcal higher than the W3X-L//QCISD/TZ values. In addition, the MN15-L/maug-TZ result has B2a-TS2 higher than B2a-TS1 by 1.39 kcal, which agrees with the conclusion drawn from the W3X-L//QCISD/VTZ calculations that B2a-TS2 makes only a minor contribution to the *syn*-CH_3CHOO + H_2O reaction. These two comparisons show that the MN15-L functional is quite reliable for describing the ACHAT reaction of *syn*-CH_3CHOO.

The MN15-L enthalpy of activation (7.84 kcal) of B2a-TS1 is 4.49 kcal higher than the MN15-L value of 3.25 kcal for B1a-TS1; this shows that the *syn*-CH_3CHOO + H_2O reaction is much slower than the CH_2OO + H_2O reaction.

For the DHAT reaction of *syn*-CH_3CHOO, Table 1 shows that the difference in enthalpy of activation at 0 K between W3X//QCISD/VTZ and W3X-L//QCISD/VTZ for transition states B2dh-TS1 and B2dh-TS2 is about 0.4 kcal, and the MUE of MN15-L/maug-TZ for the DHAT processes is 1.08 kcal. These comparisons show that the DHAT processes are more theoretically challenging than the ACHAT processes.

Although the *anti*-CH_3CHOO + H_2O reaction, like the *syn*-CH_3CHOO + H_2O and CH_2OO + H_2O reactions, has two transition state structures, in this case the difference between B3a-TS1 and B3a-TS2 enthalpic barriers is only 0.59 kcal, as calculated by W3X-L//QCISD/TZ and shown in Table 1. This may be compared to a difference of 1.36 kcal for the *syn*-CH_3CHOO case and to a difference of 0.87 kcal for the CH_2OO case; this comparison indicates that the second reaction pathway is more significant for the *anti*-CH_3CHOO case than for the other two reactions. The enthalpic barrier of B3a-TS1 is more than 6 kcal lower than that of B2a-TS1; this confirms that the *anti*-CH_3CHOO + H_2O reaction is much faster than the *syn*-CH_3CHOO + H_2O reaction, which is consistent with the experimental results in the literature.[30]

The four intermediates B2a-P1, B2a-P2, B3a-P1, and B3a-P2 must be treated as conformers rather than as separate species because the enthalpies of activations for interconversion among these conformers are below 10 kcal, as shown in Figure S18.

DOI: 10.1021/jacs.6b08655
J. Am. Chem. Soc. 2016, 138, 14409−14422

Table 3. High-Pressure Limits of MP-CVT/SCT Bimolecular Rate Constants (cm^3 $molecule^{-1}$ s^{-1}) of CH_2OO + H_2O Reaction B1a, *syn*-CH_3CHOO + H_2O Reaction B2 (Which Is the Sum of Reactions B2a and B2dh), and *anti*-CH_3CHOO + H_2O Reaction B3a and Unimolecular Rate Constants (s^{-1}) of CH_2OO (U1c), *syn*-CH_3CHOO (U2hs), and *anti*-CH_3CHOO (U3c)

T (K)	k_{B1a}	k_{U1c}	k_{B2}	k_{U2hs}	k_{B3a}	k_{U3c}
200	3.52×10^{-17}	1.05×10^{-7}	2.62×10^{-20}	5.60×10^{0}	4.24×10^{-15}	1.94×10^{-4}
220	5.82×10^{-17}	5.75×10^{-6}	3.08×10^{-20}	1.29×10^{1}	4.37×10^{-15}	5.72×10^{-3}
240	9.00×10^{-17}	1.75×10^{-4}	4.24×10^{-20}	2.93×10^{1}	4.55×10^{-15}	1.03×10^{-1}
260	1.32×10^{-16}	3.27×10^{-3}	6.67×10^{-20}	6.66×10^{1}	4.76×10^{-15}	1.22×10^{0}
280	1.84×10^{-16}	4.13×10^{-2}	1.14×10^{-19}	1.53×10^{2}	4.99×10^{-15}	1.03×10^{1}
290	2.15×10^{-16}	1.30×10^{-1}	1.51×10^{-19}	2.33×10^{2}	5.11×10^{-15}	2.69×10^{1}
297	2.38×10^{-16}	2.76×10^{-1}	1.85×10^{-19}	3.14×10^{2}	5.19×10^{-15}	5.07×10^{1}
298	2.41×10^{-16}	3.07×10^{-1}	1.90×10^{-19}	3.28×10^{2}	5.21×10^{-15}	5.54×10^{1}
300	2.48×10^{-16}	3.78×10^{-1}	2.01×10^{-19}	3.57×10^{2}	5.24×10^{-15}	6.61×10^{1}
320	3.24×10^{-16}	2.65×10^{0}	3.54×10^{-19}	8.47×10^{2}	5.49×10^{-15}	3.38×10^{2}
340	4.12×10^{-16}	1.49×10^{1}	6.07×10^{-19}	2.01×10^{3}	5.76×10^{-15}	1.43×10^{3}
350	4.61×10^{-16}	3.29×10^{1}	7.86×10^{-19}	3.09×10^{3}	5.89×10^{-15}	2.78×10^{3}

Table 4. Parameters in Fits to High-Pressure Rate Constants and Arrhenius Activation Energies

reaction	ln B^a	C (K)	D (kcal)	n	E_a (200 K) (kcal)	E_a (298 K) (kcal)
B1a	−33.493	79.846	1.412	1.524	2.15	2.51
U1c	26.623	84.963	14.030	1.454	17.21	18.54
B2[b]	92.645	246.869	46.717	−84.123	−0.70	5.13
U2hs	−58.152	990.088	44.302	62.322	3.24	7.50
B3a	−31.864	−98.918	0.889	0.296	0.10	0.43
U3c	29.898	91.210	12.682	−1.169	14.49	15.57

[a] B is in units of cm^3 $molecule^{-1}$ s^{-1}. [b] Reaction B2 is the sum of reactions B2a and B2dh.

3.4. Unimolecular Reactions of *syn*-CH_3CHOO and *anti*-CH_3CHOO. For the unimolecular reaction of *syn*-CH_3CHOO, the W3X-L calculations in Table 2 indicate that the hydrogen atom transfer process via U2hs-TS has an enthalpy of activation (17.01 kcal) that is 6.69 kcal lower than that for the oxygen atom transfer process via U2c-TS (23.70 kcal). The table also shows that the MN15-L enthalpy of activation for U2hs-TS (16.41 kcal) is reasonably consistent with the W3X-L value of 17.01 kcal and with the literature value[78] of 17.1 kcal calculated by CCSD(T)/TZ.

Figure 2 shows that water catalytically lowers the enthalpy of activation for the production of CH_2=CHOOH, which is U2hs-P, from 17.01 to 9.68 kcal.

A diagram similar to Figure 2 but for *anti*-CH_3CHOO is given in Figure S17, which shows that the dominant pathway for the unimolecular reaction of *anti*-CH_3CHOO is an oxygen atom transfer route similar to that which dominates the unimolecular reaction of CH_2OO; this route passes through U3c-TS, as depicted in Figure S17. Table 2 shows that the W3X-L enthalpy of activation through U3c-TS is 3.4 kcal lower than that through U1c-TS, so this reaction is much faster for *anti*-CH_3CHOO than for CH_2OO.

3.5. Rate Constants. The calculated rate constants in the high-pressure limit are in Table 3. In principle, all reactions studied here have pressure effects because either the reaction or its reverse (or both) is bimolecular. The high-pressure limit of the unimolecular rate constants assumes Boltzmann-equilibrated internal energy distributions of the reactants, and the high-pressure limit of reactions producing a single product assumes that the product is equilibrated before back reaction occurs. Thus, the pressure effects are nonequilibrium effects, and when they are not negligible, they decrease the rate constants below the high-pressure limit. Such nonequilibrium effects are greater at higher temperatures than at atmospheric temperatures, and indeed no pressure effect was observed in experimental studies of the bimolecular reactions considered here. We are interested in altitudes up to 50 km (the top of the stratosphere), where the pressure has dropped to 0.7×10^{-3} bar, and therefore we calculated the pressure effects for all three bimolecular reactions and all three unimolecular reactions.

Figures S19, S21, S23 show that we predict no significant pressure effect on the bimolecular reactions under the conditions of interest, and we need not discuss pressure effects on the bimolecular reactions. The pressure effects on unimolecular reactions are greater and are discussed below.

The high-pressure rate constants in Table 3 are fitted using the following four-parameter function[68] in the temperature range between 190 and 350 K

$$k = B\left(\frac{T + C}{300}\right)^{n} \exp\left[-\frac{D(T + C)}{R(T^2 + C^2)}\right] \quad (3)$$

where R is the ideal gas constant (1.9872×10^{-3} kcal mol^{-1} K^{-1}), T is temperature in K, and the parameters are in Table 4. The high-pressure Arrhenius activation energies are calculated by

$$E_a = -R\frac{d \ln k}{d(1/T)} \quad (4)$$

and they are provided at two temperatures in Table 4 and at other temperatures in Table S9.

3.5.1. CH_2OO. The rate constant of the CH_2OO + H_2O reaction (reaction B1a) is estimated to be 2.4×10^{-16} at 298 K, which is in excellent agreement with the most recent experimental result of $(3.2 \pm 1.2) \times 10^{-16}$.[77] Furthermore, the calculated value does not exceed the upper limits of 4×10^{-15} and 1.5×10^{-15} from the measurements by Welz et al.[20] and Lin et al.,[26] respectively. However, the calculated rate

DOI: 10.1021/jacs.6b08655
J. Am. Chem. Soc. 2016, 138, 14409−14422

constant (2.4×10^{-16}) does not agree with the values of 5.4×10^{-18} at 297 K,[27] $(2.5 \pm 1) \times 10^{-17}$ at 297 K,[28] $(1.3 \pm 0.4) \times 10^{-15}$ at 298 K,[29] and 1×10^{-15} at 295 K[108] from indirect kinetics measurements.

Table S10 shows the individual fractional contributions to reaction B1a through the B1a-TS1 and B1a-TS2 transition state facets, with the former accounting for 77−90% of the reaction. This is in line with the B1a-TS1 calculated reaction barrier being lower than that for B1a-TS2. The fractional contribution of B1a-TS1 to the overall rate constant decreases with increasing temperature, as expected when the branching is dominated by an enthalpic factor.

The high-pressure-limit unimolecular rate constant k_{U1c} for conversion of CH_2OO to dioxirane is strongly dependent on the temperature, as can be seen in Table 3, where the rate constant increases to 3.3×10^{1} at 350 K from 1.05×10^{-7} at 200 K. Table 3 shows that the calculated high-pressure-limit unimolecular rate constant of CH_2OO is 0.31 at 298 K, and this agrees well with the previous theoretical result of 0.3.[109] However, the finite-pressure rate constant of U1c is calculated to be only 0.072 at 298 K and 1 bar, which indicates a pressure effect of a factor of 4.3 even at temperatures this low and pressures this high. The calculated finite-pressure rate constant is smaller than the recent experimental[29] upper bound of 4 ("zero within uncertainty") at 298 K and ∼1 bar; note though that we consider the elementary rate constant of the first step of the unimolecular isomerization of CH_2OO, whereas the experiment involves the whole mechanism.

The pressure effect can be even larger at high altitudes, as shown by columns 5 and 7 of Table 5. For example, the ratio of high-pressure limit rate constant to the pressure-dependent rate constant is 3.11×10^{3} at 50 km.

Table 5. Pressure-Dependent Rate Constant and Ratio of the High-Pressure-Limit Rate Constant to the Pressure-Dependent Rate Constant for the Unimolecular Rate Constants of U1c and U3c at a Sequence of Altitudes

H^a (km)	T^a (K)	P^a (mbar)	$k_{U1c}{}^b$	$v_{U1c}{}^c$	$k_{U3c}{}^b$	$v_{U3c}{}^c$
0	288.8	1013	2.92×10^{-2}	3.90	2.02×10^{1}	1.19
5	259.3	542	6.85×10^{-4}	4.32	2.92×10^{-1}	3.84
10	229.7	269	8.40×10^{-6}	3.82	2.00×10^{-2}	1.23
15	212.6	122	3.75×10^{-7}	3.79	1.41×10^{-3}	1.24
20	215.5	55	3.00×10^{-7}	8.27	1.73×10^{-3}	1.62
25	218.6	25	2.25×10^{-7}	19.7	1.81×10^{-3}	2.55
30	223.7	11.5	2.15×10^{-7}	52.6	4.08×10^{-3}	2.48
35	235.1	5.4	4.67×10^{-7}	170	3.86×10^{-3}	13.6
40	249.9	2.7	1.48×10^{-6}	529	9.90×10^{-3}	36.7
45	266.1	1.4	4.98×10^{-6}	1480	2.59×10^{-2}	92.7
50	271.0	0.73	4.44×10^{-6}	3110	2.15×10^{-2}	189

[a] H (altitude), T (temperature), and P (pressure) are from ref 112. [b] The pressure-dependent rate constant. [c] The ratio of the high-pressure-limit rate constant to the pressure-dependent rate constant.

We also test the sensitivity of the pressure-dependent rate constant of CH_2OO to the average energy transfer per deactivating collision from 300 to 500 cm^{-1} from the previous studies of Criegee intermediates,[9,76,109] as shown in Table S11.

3.5.2. syn-CH_3CHOO. The rate constant for the *syn*-CH_3CHOO + H_2O reaction is estimated to be 1.9×10^{-19} at 298 K, which is below the experimental upper limits of 4×10^{-15} established by Taatjes et al.[30] and 2×10^{-16} established by Sheps et al.[31] The branching fraction of rate constants in the *syn*-CH_3CHOO + H_2O reaction is of great interest, and the branching factions for B2a and B2dh are provided in Figure 3,

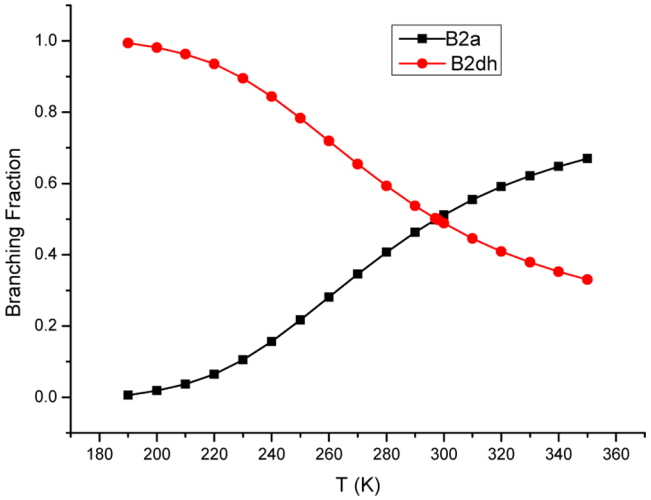

Figure 3. Branching fractions as a function of temperature.

which shows that B2dh is larger than B2a below 290 K. Tunneling transmission coefficients are listed in Table 6, which

Table 6. Tunneling Transmission Coefficients (Unitless) for Various Reaction Paths[a]

T (K)	B2a-TS1	B2a-TS2	B2dh-TS1	B2dh-TS2	U2hs-TS
200	3.14	3.19	3.36×10^{4}	7.08×10^{4}	4.13×10^{6}
220	2.46	2.48	4.58×10^{3}	8.92×10^{3}	1.89×10^{5}
240	2.07	2.09	9.96×10^{2}	1.78×10^{3}	1.65×10^{4}
260	1.83	1.84	3.08×10^{2}	5.08×10^{2}	2.37×10^{3}
280	1.67	1.67	1.24×10^{2}	1.89×10^{2}	5.14×10^{2}
290	1.60	1.61	8.53×10^{1}	1.25×10^{2}	2.72×10^{2}
297	1.57	1.57	6.72×10^{1}	9.63×10^{1}	1.82×10^{2}
298	1.56	1.57	6.50×10^{1}	9.29×10^{1}	1.73×10^{2}
300	1.55	1.56	6.10×10^{1}	8.66×10^{1}	1.55×10^{2}
320	1.46	1.47	3.46×10^{1}	4.63×10^{1}	6.14×10^{1}
330	1.43	1.43	2.72×10^{1}	3.55×10^{1}	4.20×10^{1}
350	1.37	1.37	1.80×10^{1}	2.25×10^{1}	2.25×10^{1}

[a] See Figure 2.

shows that the tunneling transmission coefficients are very large for the double hydrogen transfer process at 200 K. Furthermore, the tunneling transmission coefficient in the unimolecular reaction of *syn*-CH_3CHOO to CH_2=$CHOOH$ is even larger than the one in reaction B2dh; in particular, it is 4.1×10^{6} at 200 K, as listed in Table 6. These results show clearly that tunneling effects make an important contribution to the hydrogen transfer processes investigated here. Tunneling often contributes a large temperature dependence to the slope of an Arrhenius plot (i.e., to the Arrhenius activation energy) at low temperature, and Table 4 indeed shows that the Arrhenius activation energies of the reactions of *syn*-CH_3CHOO increase significantly with increasing temperature over the 200−298 K temperature range. Table 4 shows that increases are also found for reactions of CH_2OO and *anti*-CH_3CHOO, but they are smaller.

The unimolecular rate constant for the isomerization of *syn*-CH_3CHOO to CH_2=$CHOOH$ (reaction U2hs) is given in

DOI: 10.1021/jacs.6b08655
J. Am. Chem. Soc. 2016, 138, 14409−14422

Table 7. Corresponding Atmospheric Lifetimes (s) at Different Temperatures and Pressures[a,b]

H^b (km)	T^b (K)	P^c (mbar)	τ_{B1a}	τ_{U1c}	τ_{B2}	τ_{U2hs}	τ_{B3a}	τ_{U3c}
0	288.8	1013	1.3×10^{-2}	3.4×10^{1}	1.9×10^{1}	4.5×10^{-3}	5.6×10^{-4}	4.9×10^{-2}
5	259.3	542	5.1×10^{-1}	1.5×10^{3}	1.0×10^{3}	1.5×10^{-2}	1.4×10^{-2}	3.4×10^{0}
10	229.7	269	4.5×10^{1}	1.2×10^{5}	9.5×10^{4}	5.3×10^{-2}	7.3×10^{-1}	5.0×10^{1}
15	212.6	122	1.7×10^{3}	2.7×10^{6}	2.8×10^{6}	1.1×10^{-1}	1.9×10^{1}	7.1×10^{2}
20	215.5	55	3.2×10^{3}	3.3×10^{6}	5.7×10^{6}	9.5×10^{-2}	3.9×10^{1}	5.8×10^{2}
25	218.6	25	5.5×10^{3}	4.4×10^{6}	1.0×10^{7}	8.3×10^{-2}	7.1×10^{1}	5.5×10^{2}
30	223.7	11.5	9.7×10^{3}	4.7×10^{6}	1.9×10^{7}	6.8×10^{-2}	1.4×10^{2}	2.5×10^{2}
35	235.1	5.4	1.5×10^{4}	2.1×10^{6}	3.3×10^{7}	4.2×10^{-2}	2.7×10^{2}	2.6×10^{2}
40	249.9	2.7	2.3×10^{4}	6.8×10^{5}	4.9×10^{7}	2.3×10^{-2}	5.4×10^{2}	1.0×10^{2}
45	266.1	1.4	3.3×10^{4}	2.0×10^{5}	6.3×10^{7}	1.2×10^{-2}	1.0×10^{3}	3.9×10^{1}
50	271.0	0.73	5.7×10^{4}	2.2×10^{5}	1.0×10^{8}	9.8×10^{-3}	1.9×10^{3}	4.7×10^{1}

[a]For bimolecular reactions, $\tau_{B1a} = \frac{1}{k_{B1a}[X]}$, $\tau_{B2} = \frac{1}{k_{B2}[X]}$, and $\tau_{B3a} = \frac{1}{k_{B3a}[X]}$, where k_{B1a}, k_{B2}, and k_{B3a} are the bimolecular rate constants of reactions B1a, B2 (which is the sum of B2a and B2dh), and B3a, respectively, and $[X]$ is the concentration of H_2O. [b]For the unimolecular reactions, $\tau_{U1c} = \frac{1}{k_{U1c}}$, $\tau_{U2dh} = \frac{1}{k_{U2dh}}$, and $\tau_{U3c} = \frac{1}{k_{U3c}}$, where k_{U1c}, k_{U2hs}, and k_{U3c} are the unimolecular rate constants of reactions U1c, U2hs, and U3c, respectively. [c]H, T, and P are from ref 112.

Table 3, which shows the temperature dependence in the high-pressure limit. At 298 K, the high-pressure limit rate constant of *syn*-CH_3CHOO to CH_2=$CHOOH$ is 328, which is about 13 times larger than a previous theoretical value of 24.2,[76] which was computed with CCSD(T)-level electronic structure theory (whereas the present work used beyond-CCSD(T) electronic structure theory) and less complete dynamics, in particular the Eckart approximation[110] for tunneling. Interestingly, although the beyond-CCSD(T) effect was to raise the barrier by 0.44 kcal/mol (see Table 2), our rate constant is larger. We attribute this to a more complete treatment of the dynamics. Our SCT transmission coefficient at 298 K is 173 (in Table 6), whereas this value with the less accurate Eckart model is about 3 times smaller. (At 200 K, our rate constant is 59 times larger that that in ref 76, and most of that difference comes from our transmission coefficient being larger by a factor of 12. Note that SCT transmission coefficients depend on the shape of the vibrationally adiabatic ground-state potential energy curve $V_a^G(s)$ over a significant range of reaction coordinate s and on the reaction-path curvature as a function of s, where $V_a^G(s)$ equals the sum of the potential energy $V_{MEP}(s)$ along the minimum energy path and the local zero-point energy for motion transverse to the minimum energy path. Therefore, the SCT transmission coefficients cannot be easily interpreted using only the barrier height and the zero-point energy of the imaginary frequency of the saddle point.)

A more recent calculation[78] of the reaction rate of U2hs also used the Eckart approximation for tunneling and gave a rate constant of 166 at 298 K, about a factor of 2 smaller than our value of 328. We made a detailed analysis of whether the difference can be attributed to the different tunneling approximations; the details of this analysis are provided in Table S12, and the analysis may be summarized as follows. In old work, the Eckart potential was usually fitted to the potential energy. In modern work, including ref 78, it is often fitted to $V_a^G(s)$ at the reactants, the saddle point, and the products (which is equivalent to fitting it to ΔH_0° and $\Delta H_0^{\ddagger,\circ}$) and (somewhat inconsistently) to $\frac{\partial^2 V_{MEP}}{\partial s^2}$; therefore, this can be considered to be an approximation to zero curvature tunneling, which is based on the entire $V_a^G(s)$. At 298 K, the Eckart approximation of ref 78 is a factor of 3.8 greater than our ZCT calculation, whereas an Eckart approximation fit in the same way to the MN15-L/maug-TZ calculations is only 1.5 times large than our ZCT calculation. This illustrates the great sensitivity of the Eckart approximation to the potential energy surface. However, the error in overestimating the ZCT transmission coefficient is partly canceled by the fact that the SCT tunneling transmission coefficient is a factor of 5.8 times larger than the ZCT tunneling transmission coefficient at 298 K. Thus, a more complete treatment of the tunneling would be in the correct direction to account for the difference of the rate constant of ref 78 from the present result. In fact, the reaction path curvature cannot be neglected for a realistic treatment of this reaction at atmospheric temperatures. For example, Table S12 shows that the SCT transmission coefficient is 2.6 times larger than the ZCT one at 350 K.

Our prediction for the effect of pressure is shown in Figure S22, which shows a significant pressure effect at 350 K but a very small pressure effect at 298 K and lower.

Finally, we can compare to a recent experiment for rate constant for OH formation, which yields 17 ± 14.[35] This is considerably smaller than our calculated result, but we are considering only the first step in the mechanism, and one would have to consider the fate of vinyl hydroperoxide to compare to theoretical results to that experiment.

3.5.3. anti-CH_3CHOO. The rate constant of the reaction of *anti*-CH_3CHOO with H_2O is computed to be 5.2×10^{-15} at 298 K, which is in good agreement (factor of 2) with the experimental value of $(1.0 \pm 0.4) \times 10^{-14}$.[30]

The high-pressure limit rate constant of U3c at 298 K is 55.4, which agrees well with the previous theoretical value of 67.2.[76] However, Figure S24 shows that the unimolecular rate constant k_{U3c} is strongly dependent on both T and P, as also shown in Table 5. The transition pressure, $P_{1/2}$, is the pressure at which the unimolecular reaction has a value only one-half of the high-pressure limit. Table S13 shows that this drops from 0.3 bar at 350 K to 0.007 bar at 190 K for reaction U3c; this may compare to a drop from 16 to 0.07 bar over the same temperature range for reaction U1c, which again reinforces the large magnitude of the pressure effect for the smallest Criegee intermediate.

3.6. Atmospheric Implications. We note that the dominant removal reaction is not necessarily the only important reaction of an atmospheric species because even if X + Y is the dominant removal for X, X + Z could still be the dominant reaction for Z. The present calcuations are

DOI: 10.1021/jacs.6b08655
J. Am. Chem. Soc. 2016, 138, 14409−14422

Table 8. Rate Constants of Criegee Intermediates Reaction with H_2O and SO_2, the Concentrations of H_2O and SO_2, and the Corresponding Reaction-Specific Atmospheric Lifetimes at 298 K and at Altitude 0 km

reaction	k [ref] (cm^3 $molecule^{-1}$ s^{-1})	concentration (molecules cm^{-3})	τ^b (s)
$CH_2OO + H_2O$	2.41×10^{-16} [this work]	3.8×10^{17} [a]	0.011
syn-$CH_3CHOO + H_2O$	5.72×10^{-20} [this work]	3.8×10^{17} [a]	46.0
anti-$CH_3CHOO + H_2O$	6.32×10^{-15} [this work]	3.8×10^{17} [a]	0.0004
$CH_2OO + SO_2$	3.9×10^{-11} [20]	9×10^{10}	0.28
syn-$CH_3CHOO + SO_2$	2.4×10^{-11} [30]	9×10^{10}	0.46
anti-$CH_3CHOO + SO_2$	6.7×10^{-11} [30]	9×10^{10}	0.17

[a]Relative humidity 50%, 1 atm. [b]$\tau = \frac{1}{k[X]}$, where k and $[X]$ stand for the rate constant and the concentration of H_2O or SO_2, respectively

particularly relevant to understanding the removal of Criegee intermediates, and this section will focus on that issue.

Alkene ozonolysis to make stabilized Criegee intermediates occurs primarily in the troposphere (the concentration of organics in the stratosphere is quite low, and stabilization of Criegee intermediates would also be small at the lower pressures in the stratosphere). Furthermore, stratospheric radical chemistry is much more strongly coupled to photolytic reactions, e.g., the Chapman cycle, than to oxidation of organics. For these reasons, we focus mainly on tropospheric altitudes, i.e., altitudes up to about[111] 15−17 km.

Water concentration in the upper atmosphere is variable (with daily and seasonal fluctuations as well as systematic changes due to climate change) and is hard to estimate in a general way. For illustration purposes, we will use the estimate of Brasseur and Solomon,[112] who made estimates based on a one-dimensional radiative convective photochemical model. Their estimates nominally apply to midlatitudes at equinox, but here we just take them as one plausible scenario for a model atmosphere (sometimes called a standard atmosphere). Their estimates for the water concentration as a function of altitude are in Table S14, and an estimate obtained from another source is in Table S15. Since these estimates are similar, the next three paragraphs discuss only the situation based on the estimates in Table S14.

Table S16 gives the bimolecular and unimolecular rate constants at the combinations of pressure and temperature involved at various altitudes. From these tables, we computed the reaction-specific lifetimes with respect to bimolecular reaction with water and with respect to unimolecular reaction at the temperatures and pressures corresponding to various altitudes; the lifetimes are defined in Section 2 below eq 2, and the results are given in Table 7.

3.6.1. CH_2OO. Table 7 indicates that for CH_2OO a bimolecular reaction with H_2O is more likely than a unimolecular reaction ($\tau_{B1a} < \tau_{U1c}$).

Criegee intermediates are potentially important in the atmospheric oxidation of SO_2, which is important because it leads eventually to the formation of sulfuric acid.[12,14,16,18,113−117] The variation of SO_2 with altitude has been studied at various locations,[118] but we limit discussion to a single fairly high value corresponding to "a polluted mega-city (Mexico City)".[119] Experimental results have shown that the rate constant of the $CH_2OO + SO_2$ reaction is pressure-independent,[27] so we base our discussion of the reactions with SO_2 on the high-pressure-limit rate constants. Table 8 then shows the competition between Criegee intermediates reacting with water as compared to reaction with SO_2. This table clearly shows that even with such a high concentration of SO_2 the $CH_2OO + H_2O$ reaction is still much more likely than the reaction with SO_2.

Another important reaction to consider is the CH_2OO reaction with water dimers. Recent experimental investigations[26,39,115,120,121] have led to rate constants in the range 4−8.9 × 10^{-12} at 294−298 K;[26,120] these rate constants are about 3 × 10^4 larger than the $CH_2OO + H_2O$ rate constant; if we assume that $[(H_2O)_2]/[H_2O]$ is ∼8 × 10^{-4} as in Tables S14 and S15 or 1.0 × 10^{-3} as assumed in ref 39, then the dimer reaction is 20−30 times more probable than the monomer reaction. At 283 K, the measured dimer rate constant is 1.5 × 10^{-11}, although we note that in later work some of these authors of this measurement revised their best estimate at 298 K from 7.4 × 10^{-12} to 6.5 × 10^{-12}; applying the same factor at 283 K would yield 1.3 × 10^{-11}, which is 7 × 10^4 greater than our rate constant with for the monomer at this temperature. At 3 km, Table S15 shows a temperature close to this, and the dimer to monomer ratio is ∼4 × 10^{-4}, which makes the reaction rate with the dimer only 3 times more probable than the reaction with the monomer. As we go farther up in altitude to the tropopause (∼15−17 km), the $[(H_2O)_2]/[H_2O]$ ratio decreases by 3−4 orders of magnitude as compared to the earth's surface, and we do not know how the rate constant ratio changes because the dimer rate constant has never been measured below 283 K. When the dimer rate constant is measured or calculated reliably at lower temperature, the present monomer calculations as functions of temperature and pressure will be useful for understanding the fate of CH_2OO at higher altitude. The present results do, however, make it likely that the water monomer reaction will dominate the water dimer reaction in the higher troposphere (above 7 km).

3.6.2. syn-CH_3CHOO. For *syn*-CH_3CHOO, the unimolecular reaction is more likely than the bimolecular one ($\tau_{U2hs} \ll \tau_{B2}$).

Although the *syn*-$CH_3CHOO + H_2O$ reaction is much slower than the *syn*-$CH_3CHOO + SO_2$ reaction, the reaction-specific lifetime of *syn*-CH_3CHOO with respect to unimolecular isomerization to $CH_2{=}CHOOH$ is only about 0.003 s at 298 K (computed from Table 3), which is about 10^2 times shorter than the lifetime with respect to the *syn*-$CH_3CHOO + SO_2$ reaction (in Table 8). Additionally, the atmospheric lifetime of *syn*-CH_3CHOO is on the order of 10^{-2} s at altitudes 0−50 km (from Table 7), whereas the rate constant of the *syn*-CH_3CHOO + water dimer reaction is about 10^{-14} cm^3 $molecule^{-1}$ s^{-1},[39] which leads to an atmospheric lifetime with respect to this reaction of at least 10 s at low altitudes. This comparison would lead to the conclusion that the dominant fate of *syn*-CH_3CHOO is the unimolecular isomerization reaction. However, one complication not taken account of in the discussion so far is the reaction with ozone. Table S14 shows that the ozone concentration is close to the water concentration at altitudes over 20 km and only a factor of 5 lower at 15 km. Although theoretical methods have been used to investigate the reactions of Criegee intermediates with

DOI: 10.1021/jacs.6b08655
J. Am. Chem. Soc. 2016, 138, 14409−14422

ozone, the computational results are inconsistent.[122,123] Moreover, these reaction systems have strong multiconfigurational character, and further work is probably required to obtain reliable rate constants for the ozone reaction.

Table 8 shows that the *syn*-CH_3CHOO + H_2O reaction is much slower than the *syn*-CH_3CHOO + SO_2 reaction, whereas the previous investigation[115] indicated that the *syn*-CH_3CHOO + H_2O reaction is much faster than the *syn*-CH3CHOO + SO_2 reaction because the previous investigation is based on a much larger rate constant of *syn*-CH_3CHOO + H_2O ($<4 \times 10^{-15}$).

3.6.3. anti-CH_3CHOO. The estimated rate constant of *anti*-CH_3CHOO + $(H_2O)_2$ is about 10^{-11},[39] which is about 10^4 times larger that of the *anti*-CH_3CHOO + H_2O reaction. Since the concentration of water dimer is about 10^{-7} to 10^{-5} times lower than that of water monomer at 7−20 km, the *anti*-CH_3CHOO + H_2O reaction is expected to be more important than the reaction with water dimer at these altitudes.

Table 8 shows that even with a high assumed concentration of SO_2 the *anti*-CH_3CHOO + H_2O reaction is much faster than the corresponding reaction with SO_2. The most likely atmospheric reaction for *anti*-CH_3CHOO depends on the altitude, with the bimolecular reaction being more favorable at altitudes up to 30 km and the unimolecular reaction being more important at altitudes 30−50 km, although, as noted above, these reactions are less important in atmospheric modeling of the latter higher altitude range.

3.6.4. Further Discussion. At high altitudes in the stratosphere, the photodissociation processes of Criegee intermediates could be competitive with their bimolecular reactions. At low altitudes, Criegee intermediates can quickly react with atmospheric acids, particularly carboxylic acids and nitric acid, because experimental data show that the reactions of C1 and C2 Criegee intermediates with formic, acetic, and nitric acid approach the collision limit.[124,125] Thus, although the present work has sorted out some of the possibilities, future theoretical investigations of the reactions of Criegee intermediates with these atmospheric species will be required to draw final conclusions about the atmospheric fate of Criegee intermediates as a function of altitude.

4. CONCLUDING REMARKS

We demonstrated that electronic structure calculations on Criegee intermediates must include nondynamic correlation in order to obtain reliable barriers for calculating rate constants. We investigate the unimolecular reactions of CH_2OO, *syn*-CH_3CHOO, and *anti*-CH_3CHOO and their reactions with H_2O. The results eliminate the previous discrepancy between experiment and theory, and they show that recent advances in efficient post-CCSD(T) coupled cluster theory,[41,42] state-of-the-art exchange-correlation functionals for density functional theory,[51] and modern kinetics theory[65−68] can be used to successfully reproduce the limited experimental data. Therefore, they can also be used to predict the rate constants under a wider range of conditions where experimental data are not available. The rate constants were computed as a function of pressure over the entire range of temperatures that is important for atmospheric chemistry plus a few higher temperatures and some lower pressures; in contrast, the experimental measurements are mainly restricted to 293−298 K with little data on pressure dependence. Since our calculated rate constants have been validated against experimental data where available, they can be used at tropospheric temperatures where no experimental data are available. Thus, we see that theory, utilizing recent advances in electronic structure theory and theoretical kinetics that allow for more quantitative predictions, can fill the gap between the experimentally available data and the kinetics data that are necessary in the global modeling of climate change.

The main findings of the present study are as follows:

(1) Our calculations show that CCSD(T) calculations are not reliable for obtaining accurate barrier heights for the reactions of Criegee intermediates with H_2O. We therefore carried out beyond-CCSD(T) calculations, and we found that for the systems studied here the recently developed MN15-L exchange-correlation functional has generally good performance, which in some cases is better than CCSD(T)/CBS.

(2) We considered two different types of reaction mechanisms for the CH_2OO + H_2O and *syn*-CH_3CHOO + H_2O reactions: ACHAT and DHAT. The importance of the DHAT process has not been elucidated in previous investigations. Furthermore, although the barrier height of DHAT is about 2.5 kcal higher than that of ACHAT, the kinetics data show that the DHAT process is faster than the ACHAT process for *syn*-CH_3CHOO because of large tunneling effects. The present results have broad implications for the reactions between Criegee intermediates and atmospheric molecules, because the two reaction mechanisms we studied in this work are in competition in the reactions of Criegee intermediates with many small molecules, such as water dimer, HCOOH, HNO_3, sulfuric acid, and HO_2.

(3) The calculations show that the bimolecular rate constants are slightly dependent on temperature, whereas the unimolecular rate constants are strongly dependent on temperature. Additionally, the unimolecular rate constants of the oxygen transfer process in CH_2OO depend strongly on pressure. Because the atmospheric fates of Criegee intermediates are determined by both the rate constants and the corresponding concentrations of atmospheric species, and these both vary with altitude, the present results show that the dominant sink processes of Criegee intermediates depend on altitude. For example, at low altitude, it is more likely that CH_2OO and *anti*-CH_3CHOO react with water than with SO_2, but the opposite is true in the case of *syn*-CH_3CHOO. The reaction of Criegee intermediates with water dimer dominates the corresponding reaction with SO_2 at low altitude.[126] However, at higher tropospheric altitudes, the reactions of Criegee intermediates with H_2O are expected to dominate over the reaction with water dimer. In addition, the unimolecular isomerization reaction of *syn*-CH_3CHOO occurs much faster than the reaction of *syn*-CH_3CHOO with SO_2. In summary, the present results provide new data relevant to atmospheric mechanisms at different altitudes.

(4) The present calculations not only yield reliable rate constants but also elucidate the theoretical requirements for treating peroxyl radicals more generally. Given the importance of Criegee intermediates and their structural variety, the present results stimulate one to reconsider the reaction mechanisms and reaction kinetics of Criegee intermediates with other atmospheric molecules and radicals. Therefore, the present results have broad

DOI: 10.1021/jacs.6b08655
J. Am. Chem. Soc. 2016, 138, 14409−14422

implications in both atmospheric chemistry and computational chemistry.

■ ASSOCIATED CONTENT

Supporting Information

The Supporting Information is available free of charge on the ACS Publications website at DOI: 10.1021/jacs.6b08655.

Tables S1−S18 give vibrational scale factors, bond lengths, rotational constants, vibrational frequencies of CH_2OO, frequencies, complexation energies, classical barrier heights, energies of reaction, Arrhenius activation energies, branching ratios, rate constants for various, average energy transfer per deactivating collision, transition pressures, concentrations of atmospheric species, rate constants, Cartesian coordinates of optimized structures, and absolute energies in hartrees. Figures S1−S15 give potential energy profiles along minimum-energy paths, and Figures S16−S18 give vibrational adiabatic ground-state potential energy curves (these are equivalent to enthalpy of activation profiles at 0 K). Figures S19−S24 give bimolecular and unimolecular rate constants as functions of temperature and pressure (PDF)

■ AUTHOR INFORMATION

Corresponding Author

*truhlar@umn.edu

Notes

The authors declare no competing financial interest.

■ ACKNOWLEDGMENTS

This work was supported in part by the U.S. Department of Energy, Office of Science, Office of Basic Energy Sciences, under Award Number DE-SC0015997, by the Science and Technology Foundation of Guizhou Province & Guizhou Minzu University, China ([2014]7380), by the Science and Technology Foundation of Guizhou Provincial Department of Education, China (No. [2015]350), and by the China Scholarship Fund.

■ REFERENCES

(1) Criegee, R. *Angew. Chem., Int. Ed. Engl.* **1975**, *14*, 745−752.
(2) Johnson, D.; Marston, G. *Chem. Soc. Rev.* **2008**, *37*, 699−716.
(3) Vereecken, L. *Science* **2013**, *340*, 154−155.
(4) Taatjes, C. A.; Shallcross, D. E.; Percival, C. J. *Phys. Chem. Chem. Phys.* **2014**, *16*, 1704−1718.
(5) Donahue, N. M.; Drozd, G. T.; Epstein, S. A.; Presto, A. A.; Kroll, J. H. *Phys. Chem. Chem. Phys.* **2011**, *13*, 10848−10857.
(6) Vereecken, L.; Francisco, J. S. *Chem. Soc. Rev.* **2012**, *41*, 6259−6293.
(7) Paulson, S. E.; Chung, M. Y.; Hasson, A. S. *J. Phys. Chem. A* **1999**, *103*, 8125−8138.
(8) Kroll, J. H.; Clarke, J. S.; Donahue, N. M.; Anderson, J. G. *J. Phys. Chem. A* **2001**, *105*, 1554−1560.
(9) Kroll, J. H.; Sahay, S. R.; Anderson, J. G.; Demerjian, K. L.; Donahue, N. M. *J. Phys. Chem. A* **2001**, *105*, 4446−4457.
(10) Sakamoto, Y.; Inomata, S.; Hirokawa, J. *J. Phys. Chem. A* **2013**, *117*, 12912−12921.
(11) Heaton, K. J.; Sleighter, R. L.; Hatcher, P. G.; Hall, W. A., IV; Johnston, M. V. *Environ. Sci. Technol.* **2009**, *43*, 7797−7802.
(12) Mauldin Iii, R. L.; Berndt, T.; Sipila, M.; Paasonen, P.; Petaja, T.; Kim, S.; Kurten, T.; Stratmann, F.; Kerminen, V. M.; Kulmala, M. *Nature* **2012**, *488*, 193−196.
(13) Boy, M.; Mogensen, D.; Smolander, S.; Zhou, L.; Nieminen, T.; Paasonen, P.; Plass-Dülmer, C.; Sipilä, M.; Petäjä, T.; Mauldin, L.; Berresheim, H.; Kulmala, M. *Atmos. Chem. Phys.* **2013**, *13*, 3865−3879.
(14) Percival, C. J.; Welz, O.; Eskola, A. J.; Savee, J. D.; Osborn, D. L.; Topping, D. O.; Lowe, D.; Utembe, S. R.; Bacak, A.; McFiggans, G.; Cooke, M. C.; Xiao, P.; Archibald, A. T.; Jenkin, M. E.; Derwent, R. G.; Riipinen, I.; Mok, D. W. K.; Lee, E. P. F.; Dyke, J. M.; Taatjes, C. A.; Shallcross, D. E. *Faraday Discuss.* **2013**, *165*, 45−73.
(15) Sarwar, G.; Simon, H.; Fahey, K.; Mathur, R.; Goliff, W. S.; Stockwell, W. R. *Atmos. Environ.* **2014**, *85*, 204−214.
(16) Berndt, T.; Jokinen, T.; Mauldin, R. L.; Petäjä, T.; Herrmann, H.; Junninen, H.; Paasonen, P.; Worsnop, D. R.; Sipilä, M. *J. Phys. Chem. Lett.* **2012**, *3*, 2892−2896.
(17) Pierce, J. R.; Evans, M. J.; Scott, C. E.; D'Andrea, S. D.; Farmer, D. K.; Swietlicki, E.; Spracklen, D. V. *Atmos. Chem. Phys.* **2013**, *13*, 3163−3176.
(18) Ahrens, J.; Carlsson, P. T. M.; Hertl, N.; Olzmann, M.; Pfeifle, M.; Wolf, J. L.; Zeuch, T. *Angew. Chem., Int. Ed.* **2014**, *53*, 715−719.
(19) Taatjes, C. A.; Meloni, G.; Selby, T. M.; Trevitt, A. J.; Osborn, D. L.; Percival, C. J.; Shallcross, D. E. *J. Am. Chem. Soc.* **2008**, *130*, 11883−11885.
(20) Welz, O.; Savee, J. D.; Osborn, D. L.; Vasu, S. S.; Percival, C. J.; Shallcross, D. E.; Taatjes, C. A. *Science* **2012**, *335*, 204−207.
(21) Su, Y.-T.; Huang, Y.-H.; Witek, H. A.; Lee, Y.-P. *Science* **2013**, *340*, 174−176.
(22) Womack, C. C.; Martin-Drumel, M.-A.; Brown, G. G.; Field, R. W.; McCarthy, M. C. *Science Advances* **2015**, *1*, e1400105.
(23) Lin, H.-Y.; Huang, Y.-H.; Wang, X.; Bowman, J. M.; Nishimura, Y.; Witek, H. A.; Lee, Y.-P. *Nat. Commun.* **2015**, *6*, 7012.
(24) Lee, Y.-P. *J. Chem. Phys.* **2015**, *143*, 020901.
(25) Osborn, D. L.; Taatjes, C. A. *Int. Rev. Phys. Chem.* **2015**, *34*, 309−360.
(26) Chao, W.; Hsieh, J.-T.; Chang, C.-H.; Lin, J. J.-M. *Science* **2015**, *347*, 751−754.
(27) Stone, D.; Blitz, M.; Daubney, L.; Howes, N. U. M.; Seakins, P. *Phys. Chem. Chem. Phys.* **2014**, *16*, 1139−1149.
(28) Ouyang, B.; McLeod, M. W.; Jones, R. L.; Bloss, W. J. *Phys. Chem. Chem. Phys.* **2013**, *15*, 17070−17075.
(29) Newland, M. J.; Rickard, A. R.; Alam, M. S.; Vereecken, L.; Munoz, A.; Rodenas, M.; Bloss, W. J. *Phys. Chem. Chem. Phys.* **2015**, *17*, 4076−4088.
(30) Taatjes, C. A.; Welz, O.; Eskola, A. J.; Savee, J. D.; Scheer, A. M.; Shallcross, D. E.; Rotavera, B.; Lee, E. P. F.; Dyke, J. M.; Mok, D. K. W.; Osborn, D. L.; Percival, C. J. *Science* **2013**, *340*, 177−180.
(31) Sheps, L.; Scully, A. M.; Au, K. *Phys. Chem. Chem. Phys.* **2014**, *16*, 26701−26706.
(32) Chhantyal-Pun, R.; Davey, A.; Shallcross, D. E.; Percival, C. J.; Orr-Ewing, A. J. *Phys. Chem. Chem. Phys.* **2015**, *17*, 3617−3626.
(33) Sheps, L. *J. Phys. Chem. Lett.* **2013**, *4*, 4201−4205.
(34) Buras, Z. J.; Elsamra, R. M. I.; Green, W. H. *J. Phys. Chem. Lett.* **2014**, *5*, 2224−2228.
(35) Novelli, A.; Vereecken, L.; Lelieveld, J.; Harder, H. *Phys. Chem. Chem. Phys.* **2014**, *16*, 19941−19951.
(36) Anglada, J. M.; Gonzalez, J.; Torrent-Sucarrat, M. *Phys. Chem. Chem. Phys.* **2011**, *13*, 13034−13045.
(37) Vereecken, L.; Glowacki, D. R.; Pilling, M. J. *Chem. Rev.* **2015**, *115*, 4063−4114.
(38) Long, B.; Tan, X.-F.; Long, Z.-W.; Wang, Y.-B.; Ren, D.-S.; Zhang, W.-J. *J. Phys. Chem. A* **2011**, *115*, 6559−6567.
(39) Lin, L.-C.; Chang, H.-T.; Chang, C.-H.; Chao, W.; Smith, M. C.; Chang, C.-H.; Jr-Min Lin, J.; Takahashi, K. *Phys. Chem. Chem. Phys.* **2016**, *18*, 4557−4568.
(40) Raghavachari, K.; Trucks, G. W.; Pople, J. A.; Head-Gordon, M. *Chem. Phys. Lett.* **1989**, *157*, 479−483.
(41) Chan, B.; Radom, L. *J. Chem. Theory Comput.* **2013**, *9*, 4769−4778.
(42) Chan, B.; Radom, L. *J. Chem. Theory Comput.* **2015**, *11*, 2109−2119.

DOI: 10.1021/jacs.6b08655
J. Am. Chem. Soc. 2016, 138, 14409−14422

(43) Kumar, M.; Sinha, A.; Francisco, J. S. *Acc. Chem. Res.* **2016**, *49*, 877−883.
(44) Lee, T. J.; Scuseria, G. E. In *Quantum Mechanical Electronic Structure Calculations with Chemical Accuracy*; Langhoff, S. R., Ed.; Kluwer: Dordrecht, 1995; pp 47−108.
(45) Adler, T. B.; Knizia, G.; Werner, H.-J. *J. Chem. Phys.* **2007**, *127*, 221106.
(46) Knizia, G.; Adler, T. B.; Werner, H.-J. *J. Chem. Phys.* **2009**, *130*, 054104.
(47) Peterson, K. A.; Adler, T. B.; Werner, H.-J. *J. Chem. Phys.* **2008**, *128*, 084102.
(48) Pople, J. A.; Head-Gordon, M.; Raghavachari, K. *J. Chem. Phys.* **1987**, *87*, 5968−5975.
(49) Dunning, T. H., Jr. *J. Chem. Phys.* **1989**, *90*, 1007−1023.
(50) Peterson, K. A.; Adler, T. B.; Werner, H.-J. *J. Chem. Phys.* **2008**, *128*, 084102.
(51) Yu, H. S.; He, X.; Truhlar, D. G. *J. Chem. Theory Comput.* **2016**, *12*, 1280−1293.
(52) Peverati, R.; Truhlar, D. G. *J. Phys. Chem. Lett.* **2012**, *3*, 117−124.
(53) Zhao, Y.; Truhlar, D. *Theor. Chem. Acc.* **2008**, *120*, 215−241.
(54) Lynch, B. J.; Zhao, Y.; Truhlar, D. G. *J. Phys. Chem. A* **2003**, *107*, 1384−1388.
(55) Papajak, E.; Leverentz, H. R.; Zheng, J.; Truhlar, D. G. *J. Chem. Theory Comput.* **2009**, *5*, 1197−1202.
(56) Frisch, M. J.; Trucks, G. W.; Schlegel, H. B.; Scuseria, G. E.; Robb, M. A.; Cheeseman, J. R.; Scalmani, G.; Barone, V.; Mennucci, B.; Petersson, G. A.; Nakatsuji, H.; Caricato, M.; Li, X.; Hratchian, H. P.; Izmaylov, A. F.; Bloino, J.; Zheng, G.; Sonnenberg, J. L.; Hada, M.; Ehara, M.; Toyota, K.; Fukuda, R.; Hasegawa, J.; Ishida, M.; Nakajima, T.; Honda, Y.; Kitao, O.; Nakai, H.; Vreven, T.; Montgomery, J. A., Jr.; Peralta, J. E.; Ogliaro, F.; Bearpark, M.; Heyd, J. J.; Brothers, E.; Kudin, K. N.; Staroverov, V. N.; Kobayashi, R.; Normand, J.; Raghavachari, K.; Rendell, A.; Burant, J. C.; Iyengar, S. S.; Tomasi, J.; Cossi, M.; Rega, N.; Millam, J. M.; Klene, M.; Knox, J. E.; Cross, J. B.; Bakken, V.; Adamo, C.; Jaramillo, J.; Gomperts, R.; Stratmann, R. E.; Yazyev, O.; Austin, A. J.; Cammi, R.; Pomelli, C.; Ochterski, J. W.; Martin, R. L.; Morokuma, K.; Zakrzewski, V. G.; Voth, G. A.; Salvador, P.; Dannenberg, J. J.; Dapprich, S.; Daniels, A. D.; Farkas, O.; Foresman, J. B.; Ortiz, J. V.; Cioslowski, J.; Fox, D. J. *Gaussian 09*, revision C.01; Gaussian, Inc.: Wallingford, CT, 2010.
(57) Zhao, Y.; Peverati, R.; Tang, K.; Luo, S.; Yu, H. S.; He, X.; Truhlar, D. G. *MN-GFM 6.7*; Department of Chemistry, University of Minnesota: Minneapolis, MN, 2015.
(58) Werner, H.-J.; Knowles, P. J.; Knizia, G.; Manby, F. R.; Schütz, M.; Celani, P.; Korona, T.; Lindh, R.; Mitrushenkov, A.; Rauhut, G.; Shamasundar, K. R.; Adler, T. B.; Amos, R. D.; Bernhardsson, A.; Berning, A.; Cooper, D. L.; Deegan, M. J. O.; Dobbyn, A. J.; Eckert, F.; Goll, E.; Hampel, C.; Hesselmann, A.; Hetzer, G.; Hrenar, T.; Jansen, G.; Köppl, C.; and, Y. L.; Lloyd, A. W.; Mata, R. A.; May, A. J.; McNicholas, S. J.; Meyer, W.; Mura, M. E.; Nicklass, A.; O'Neill, D. P.; Palmieri, P.; Peng, D.; Pflüger, K.; Pitzer, R.; Reiher, M.; Shiozaki, T.; Stoll, H.; Stone, A. J.; Tarroni, R.; Thorsteinsson, T.; Wang, M. *MOLPRO*, version 2012.1, a package of ab initio programs.
(59) Rolik, Z.; Szegedy, L.; Ladjánszki, I.; Ladóczki, B.; Kállay, M. *J. Chem. Phys.* **2013**, *139*, 094105.
(60) Kállay, M.; Rolik, Z.; Ladjánszki, I.; Szegedy, L.; Ladóczki, B.; Csontos, J.; Kornis, B. *MRCC, A Quantum Chemical Program Suite*. http://www.mrcc.hu/.
(61) Alecu, I. M.; Zheng, J.; Zhao, Y.; Truhlar, D. G. *J. Chem. Theory Comput.* **2010**, *6*, 2872−2887.
(62) Zheng, J.; Yu, T.; Papajak, E.; Alecu, I. M.; Mielke, S. L.; Truhlar, D. G. *Phys. Chem. Chem. Phys.* **2011**, *13*, 10885−10907.
(63) Zheng, J.; Mielke, S. L.; Clarkson, K. L.; Truhlar, D. G. *Comput. Phys. Commun.* **2012**, *183*, 1803−1812.
(64) Zheng, J.; Meana-Pañeda, R.; Truhlar, D. G. *Comput. Phys. Commun.* **2013**, *184*, 2032−2033.
(65) Zheng, J.; Truhlar, D. G. *J. Chem. Theory Comput.* **2013**, *9*, 1356−1367.
(66) Liu, Y.-P.; Lynch, G. C.; Truong, T. N.; Lu, D.-h.; Truhlar, D. G.; Garrett, B. C. *J. Am. Chem. Soc.* **1993**, *115*, 2408−2415.
(67) Yu, T.; Zheng, J.; Truhlar, D. G. *J. Phys. Chem. A* **2012**, *116*, 297−308.
(68) Zheng, J.; Truhlar, D. G. *Faraday Discuss.* **2012**, *157*, 59−88.
(69) Bao, J. L.; Meana-Paneda, R.; Truhlar, D. G. *Chem. Sci.* **2015**, *6*, 5866−5881.
(70) Bao, J. L.; Sripa, P.; Truhlar, D. G. *Phys. Chem. Chem. Phys.* **2016**, *18*, 1032−1041.
(71) Zheng, J.; Zhang, S.; Lynch, B. J.; Corchado, J. C.; Chuang, Y.-Y.; Fast, P. L.; Hu, W.-P.; Liu, Y.-P.; Lynch, G. C.; Nguyen, K. A.; Jackels, C. F.; Fernandez-Ramos, A.; Ellingson, B. A.; Melissas, V. S.; Villa, J.; Rossi, I.; Coitino, L.; Pu, J.; Albu, T. V.; Steckler, R.; Garrett, B. C.; Issacson, A. D.; Truhlar, D. G. *POLYRATE*, version 2010-A; University of Minnesota: Minneapolis, MN, 2013.
(72) Zheng, J.; Zhang, S.; Corchado, J. C.; Chuang, Y.-Y.; Coitiño, E. L.; Ellingson, B. A.; Truhlar, D. G. *GAUSSRATE*, version 2009-A; University of Minnesota: Minneapolis, MN, 2009.
(73) Bao, J. L.; Zheng, J.; Truhlar, D. G. *J. Am. Chem. Soc.* **2016**, *138*, 2690−2704.
(74) Bao, J. L.; Truhlar, D. G. *Phys. Chem. Chem. Phys.* **2016**, *18*, 10097−10108.
(75) Bao, J. L.; Zhang, X.; Truhlar, D. G. *Phys. Chem. Chem. Phys.* **2016**, *18*, 16659−16670.
(76) Kuwata, K. T.; Hermes, M. R.; Carlson, M. J.; Zogg, C. K. *J. Phys. Chem. A* **2010**, *114*, 9192−9204.
(77) Berndt, T.; Kaethner, R.; Voigtlander, J.; Stratmann, F.; Pfeifle, M.; Reichle, P.; Sipila, M.; Kulmala, M.; Olzmann, M. *Phys. Chem. Chem. Phys.* **2015**, *17*, 19862−19873.
(78) Fang, Y.; Liu, F.; Barber, V. P.; Klippenstein, S. J.; McCoy, A. B.; Lester, M. I. *J. Chem. Phys.* **2016**, *144*, 061102.
(79) Troe, J. *J. Phys. Chem.* **1979**, *83*, 114−126.
(80) Wadt, W. R.; Goddard, W. A. *J. Am. Chem. Soc.* **1975**, *97*, 3004−3021.
(81) Cremer, D.; Gauss, J.; Kraka, E.; Stanton, J. F.; Bartlett, R. J. *Chem. Phys. Lett.* **1993**, *209*, 547−556.
(82) Anglada, J. M.; Bofill, J. M.; Olivella, S.; Solé, A. *J. Am. Chem. Soc.* **1996**, *118*, 4636−4647.
(83) Miliordos, E.; Xantheas, S. S. *Angew. Chem., Int. Ed.* **2016**, *55*, 1015−1019.
(84) Daly, A. M.; Drouin, B. J.; Yu, S. *J. Mol. Spectrosc.* **2014**, *297*, 16−20.
(85) Li, J.; Carter, S.; Bowman, J. M.; Dawes, R.; Xie, D.; Guo, H. *J. Phys. Chem. Lett.* **2014**, *5*, 2364−2369.
(86) McCarthy, M. C.; Cheng, L.; Crabtree, K. N.; Martinez, O.; Nguyen, T. L.; Womack, C. C.; Stanton, J. F. *J. Phys. Chem. Lett.* **2013**, *4*, 4133−4139.
(87) Nakajima, M.; Endo, Y. *J. Chem. Phys.* **2013**, *139*, 101103.
(88) Hasson, A. S.; Chung, M. Y.; Kuwata, K. T.; Converse, A. D.; Krohn, D.; Paulson, S. E. *J. Phys. Chem. A* **2003**, *107*, 6176−6182.
(89) Ryzhkov, A. B.; Ariya, P. A. *Phys. Chem. Chem. Phys.* **2004**, *6*, 5042−5050.
(90) Nakajima, M.; Endo, Y. *J. Chem. Phys.* **2014**, *140*, 134302.
(91) Lledós, A.; Bertran, J. *J. Mol. Struct.: THEOCHEM* **1984**, *107*, 233−238.
(92) Zielinski, T. J.; Poirier, R. A. *J. Comput. Chem.* **1984**, *5*, 466−470.
(93) Yamabe, T.; Yamashita, K.; Kaminoyama, M.; Koizumi, M.; Tachibana, A.; Fukui, K. *J. Phys. Chem.* **1984**, *88*, 1459−1463.
(94) Nguyen, K. A.; Gordon, M. S.; Truhlar, D. G. *J. Am. Chem. Soc.* **1991**, *113*, 1596−1600.
(95) Long, B.; Long, Z.-W.; Wang, Y.-B.; Tan, X.-F.; Han, Y.-H.; Long, C.-Y.; Qin, S.-J.; Zhang, W.-J. *ChemPhysChem* **2012**, *13*, 323−329.
(96) Hazra, M. K.; Sinha, A. *J. Am. Chem. Soc.* **2011**, *133*, 17444−17453.
(97) Kumar, M.; Busch, D. H.; Subramaniam, B.; Thompson, W. H. *Phys. Chem. Chem. Phys.* **2014**, *16*, 22968−22973.

DOI: 10.1021/jacs.6b08655
J. Am. Chem. Soc. 2016, 138, 14409−14422

(98) Torrent-Sucarrat, M.; Francisco, J. S.; Anglada, J. M. *J. Am. Chem. Soc.* **2012**, *134*, 20632−20644.
(99) Buszek, R. J.; Sinha, A.; Francisco, J. S. *J. Am. Chem. Soc.* **2011**, *133*, 2013−2015.
(100) Nguyen, T. L.; Lee, H.; Matthews, D. A.; McCarthy, M. C.; Stanton, J. F. *J. Phys. Chem. A* **2015**, *119*, 5524−5533.
(101) Nakajima, M.; Endo, Y. *J. Chem. Phys.* **2014**, *140*, 011101.
(102) Nakajima, M.; Yue, Q.; Endo, Y. *J. Mol. Spectrosc.* **2015**, *310*, 109−112.
(103) Lynch, B. J.; Truhlar, D. G. *J. Phys. Chem. A* **2003**, *107*, 3898−3906.
(104) Bowman, J. M.; Wang, X.; Homayoon, Z. *J. Mol. Spectrosc.* **2015**, *311*, 2−11.
(105) Liu, F.; Beames, J. M.; Petit, A. S.; McCoy, A. B.; Lester, M. I. *Science* **2014**, *345*, 1596−1598.
(106) Smith, M. C.; Chao, W.; Takahashi, K.; Boering, K. A.; Lin, J. J.-M. *J. Phys. Chem. A* **2016**, *120*, 4789−4798.
(107) Kidwell, N. M.; Li, H.; Wang, X.; Bowman, J. M.; Lester, M. I. *Nat. Chem.* **2016**, *8*, 509−514.
(108) Nguyen, T. B.; Tyndall, G. S.; Crounse, J. D.; Teng, A. P.; Bates, K. H.; Schwantes, R. H.; Coggon, M. M.; Zhang, L.; Feiner, P.; Millller, D. O.; Skog, K. M.; Rivera-Rios, J. C.; Dorris, M.; Olson, K. F.; Koss, A.; Wild, R. J.; Brown, S. S.; Goldstein, A. H.; de Gouw, J. A.; Brune, W. H.; Keutsch, F. N.; Seinfeld, J. H.; Wennberg, P. O. *Phys. Chem. Chem. Phys.* **2016**, *18* (15), 10241−10254.
(109) Olzmann, M.; Kraka, E.; Cremer, D.; Gutbrod, R.; Andersson, S. *J. Phys. Chem. A* **1997**, *101* (49), 9421−9429.
(110) Garrett, B. C.; Truhlar, D. G. *J. Phys. Chem.* **1979**, *83* (22), 2921−2926.
(111) Finlayson-Pitts, B. J.; Pitts, J. N., Jr. *Chemistry of the Upper and Lower Atmosphere*; Academic Press: San Diego, CA, 2000; pp 1−14.
(112) Brasseur, G.; Solomon, S. *Aeronomy of the Middle Atmosphere: Chemistry and Physics of the Stratosphere and Mesosphere*; Springer Netherlands: Dordrecht, 1986.
(113) Sipilä, M.; Jokinen, T.; Berndt, T.; Richters, S.; Makkonen, R.; Donahue, N. M.; Mauldin Iii, R. L.; Kurtén, T.; Paasonen, P.; Sarnela, N.; Ehn, M.; Junninen, H.; Rissanen, M. P.; Thornton, J.; Stratmann, F.; Herrmann, H.; Worsnop, D. R.; Kulmala, M.; Kerminen, V. M.; Petäjä, T. *Atmos. Chem. Phys.* **2014**, *14*, 12143−12153.
(114) Berndt, T.; Jokinen, T.; Sipilä, M.; Mauldin, R. L.; Herrmann, H.; Stratmann, F.; Junninen, H.; Kulmala, M. *Atmos. Environ.* **2014**, *89*, 603−612.
(115) Huang, H.-L.; Chao, W.; Lin, J. J.-M. *Proc. Natl. Acad. Sci. U. S. A.* **2015**, *112*, 10857−10862.
(116) Kim, S.; Guenther, A.; Lefer, B.; Flynn, J.; Griffin, R.; Rutter, A. P.; Gong, L.; Cevik, B. K. *Environ. Sci. Technol.* **2015**, *49*, 3383−3391.
(117) Kuwata, K. T.; Guinn, E. J.; Hermes, M. R.; Fernandez, J. A.; Mathison, J. M.; Huang, K. *J. Phys. Chem. A* **2015**, *119*, 10316−10335.
(118) Andreae, M. O.; Berresheim, H.; Andreae, T. W.; Kritz, M. A.; Bates, T. S.; Merrill, J. T. *J. Atmos. Chem.* **1988**, *6*, 149−173.
(119) Vereecken, L.; Harder, H.; Novelli, A. *Phys. Chem. Chem. Phys.* **2012**, *14*, 14682−14695.
(120) Lewis, T. R.; Blitz, M. A.; Heard, D. E.; Seakins, P. W. *Phys. Chem. Chem. Phys.* **2015**, *17*, 4859−4863.
(121) Smith, M. C.; Chang, C.-H.; Chao, W.; Lin, L.-C.; Takahashi, K.; Boering, K. A.; Lin, J. J.-M. *J. Phys. Chem. Lett.* **2015**, *6*, 2708−2713.
(122) Kjaergaard, H. G.; Kurtén, T.; Nielsen, L. B.; Jørgensen, S.; Wennberg, P. O. *J. Phys. Chem. Lett.* **2013**, *4*, 2525−2529.
(123) Vereecken, L.; Harder, H.; Novelli, A. *Phys. Chem. Chem. Phys.* **2014**, *16*, 4039−4049.
(124) Welz, O.; Eskola, A. J.; Sheps, L.; Rotavera, B.; Savee, J. D.; Scheer, A. M.; Osborn, D. L.; Lowe, D.; Murray Booth, A.; Xiao, P.; Khan, M. A. H.; Percival, C. J.; Shallcross, D. E.; Taatjes, C. A. *Angew. Chem., Int. Ed.* **2014**, *53*, 4547−4550.
(125) Foreman, E. S.; Kapnas, K. M.; Murray, C. *Angew. Chem., Int. Ed.* **2016**, *55*, 10419−10422.
(126) Berndt, T.; Voigtlander, J.; Stratmann, F.; Junninen, H.; Mauldin Iii, R. L.; Sipila, M.; Kulmala, M.; Herrmann, H. *Phys. Chem. Chem. Phys.* **2014**, *16*, 19130−19136.

DOI: 10.1021/jacs.6b08655
J. Am. Chem. Soc. 2016, 138, 14409−14422